Sustainable Energy & Fuels

Interdisciplinary research for the development of sustainable energy technologies

Accepted Manuscript

This article can be cited before page numbers have been issued, to do this please use: F. Mantei, R. E. Ali, C. Baensch, S. Voelker, P. Haltenort, J. Burger, R. Dietrich, N. von der Assen, A. Schaadt, J. Sauer and O. Salem, *Sustainable Energy Fuels*, 2021, DOI: 10.1039/D1SE01270C.

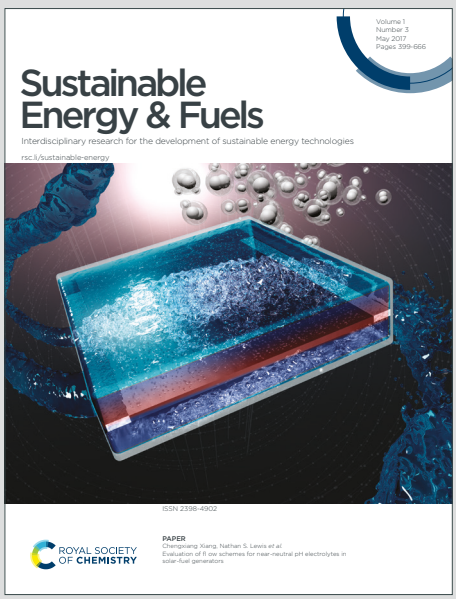

ROYAL SOCIETY OF CHEMISTRY

rsc.li/sustainable-energy

Sustainable Energy & Fuels

ROYAL SOCIETY OF CHEMISTRY View Article Online
DOI: 10.1039/D1SE01270C

PAPER

Techno-economic assessment and carbon footprint of processes for the large-scale production of oxymethylene dimethyl ethers from carbon dioxide and hydrogen

Received 00th January 20xx,
Accepted 00th January 20xx

DOI: 10.1039/x0xx00000x

Franz Mantei [a], Ramy E. Ali [a], Cornelie Baensch [b], Simon Voelker [c], Philipp Haltenort [d], Jakob Burger [e], Ralph-Uwe Dietrich [b], Niklas von der Assen [c], Achim Schaadt [a], Jörg Sauer [d] and Ouda Salem [a]*

Poly(oxymethylene) dimethyl ethers (OME) show promising fuel properties enabling drop-in into the existing infrastructure, especially as an alternative or additive to diesel fuel leading to a significant reduction in local emissions (e.g. soot, NO_x). Additionally, OME can be produced from methanol enabling a production based on renewable feedstock which can significantly reduce the carbon footprint in comparison to fossil alternatives. However, an industrial process to sustainably produce OME on a large-scale is not yet developed. Based on the results of detailed simulations in Aspen Plus® this work compares the most viable process routes for the production of OME_{3-5} in a system boundary including H_2 via water electrolysis and captured CO_2 from point sources or ultimately using direct air capture technologies. One of the main outcomes of this work is the standardized methodology introduced for the techno-economic and CO_2 footprint evaluation and comparison of such diverse processes. The comparison criteria are based on systematic approaches covering process material and energy efficiency, Technology Readiness Level, costs, and the carbon footprint. Process routes based on anhydrous formaldehyde and methanol or methylal feedstock show higher energy efficiencies and lower carbon footprints than other routes considering commercial aqueous formaldehyde. However, anhydrous formaldehyde synthesis is under research and development and not yet industrially established. Importantly, considering the net production costs of OME_{3-5} from the four simulated process routes there is no significant difference which is a consequence of the rather high share of the operational cost and specifically the costs for the feedstock H_2 and CO_2. Using sensitivity analysis, the influence of feedstock costs and carbon footprint on the evaluation criteria is identified elaborating the potential of feasible and sustainable OME production under favoured conditions.

1. Introduction

The CO_2 emission reduction targets of the German federal government in the mobility sector were achieved in 2020 according to the German environment agency (UBA) report with 19 million ton reduction to reach overall 146 million ton of CO_2-eq emissions. Nevertheless, this was correlated to COVID-19 pandemic and the mobility sector is behind its CO_2 emission reduction targets in the last two decades.[1] This sector is imposed to significantly reduce its global (mainly CO_2) and local emissions specially under the EURO 6 (NO_x< 0.08 g/km, PM< 0.0045 g/km) and the upcoming stricter EURO 7 emission reduction standards.[2] Diesel engines are currently one of the major dominant internal combustion engines used in the mobility sector[3,4] with their share expected to grow in various mobility sector modes (passenger vehicles, road freight, ships, etc.). An expected oil demand increase for passenger vehicles from 20 million barrel/d in 2020 to 27.5 mb/d in 2030 is reported by the international energy agency (IEA) study in 2020.[5] Beside combustion engine optimization and the already complex exhaust gas system improvements, altering the active combustion substance (fuel) is one of the most effective strategies to achieve these emission reduction targets.

Poly(oxymethylene) dimethyl ethers with the chemical formula $H_3C{-}(O{-}CH_2)_n{-}O{-}CH_3$ with n ≥ 2 (denoted hereon as OME) can be blended with diesel fuel or applied as neat fuel in diesel combustion engines, resulting in significant local emission reductions (i.e. Soot, NO_x). This is due to the chemical structure of OME with no direct C-C bond, high intermolecular oxygen content and the favourable fuel properties. This also enables using the existing infrastructure for transportation, storage, and distribution for OME blends with diesel.[6–9] The well-to-wheel (WtW) CO_2 emissions could be significantly reduced compared to fossil-based fuels if OME are produced from renewable carbon sources and low-carbon H_2.[10]

[a] Thermochemical Processes Department, Division Hydrogen Technologies, Fraunhofer Institute for Solar Energy Systems, Heidenhofstr. 2, 79110, Freiburg, Germany. Email: ouda.salem@ise.fraunhofer.de
[b] Energy System Integration, Institute of Engineering Thermodynamics, German Aerospace Center, Pfaffenwaldring 38-40, 70569, Stuttgart, Germany
[c] Institute of Technical Thermodynamics, Energy Systems Engineering, RWTH Aachen University, Schinkelstraße 8, 52062 Aachen, Germany
[d] Institute of Catalysis Research and Technology, Karlsruhe Institute of Technology, Hermann-von-Helmholtz-Platz 1, 76344, Eggenstein-Leopoldshafen, Germany
[e] Chemical Process Engineering, Technical University of Munich, Uferstraße 53, 94315, Straubing, Germany

† Electronic Supplementary Information (ESI) available: [details of any supplementary information available should be included here]. See DOI: 10.1039/x0xx00000x

View Article Online
DOI: 10.1039/D1SE01270C

Several studies investigated different blends of OME with diesel fuel to conform with the EN590 standard and showed significant reduction in local emissions for both heavy duty and passenger cars.[11–24] Under certain conditions even a mixture of 10 vol.-% OME with diesel can lead to significant NO_x and soot emissions reduction.[12] A stoichiometric evaluation shows that already 10 vol.-% OME blend with diesel will correspond to ca. 441 billion litres (diesel equivalent) per year OME production capacity worldwide and ca. 7.58 billion litres per year for Germany; that emphasizes the need for large-scale production plants also in blending cases. Various blending rates were investigated in heavy duty and passenger car engines by several researchers showing a significant potential to increase the engine efficiency by increasing the exhaust gas recirculation (EGR) as a consequence of overcoming the NO_x and soot trade-off.[25–27]

Importantly, life cycle assessment (LCA) studies showed the potential of CO_2 reduction based on neat OME or blends with fossil or Fischer Tropsch diesel. For a certain case study using neat OME_{3-5}, Hank et al. evaluated that the WtW greenhouse gas emissions (GHGE) can be reduced by 86%, corresponding to 29 g(CO_2-eq) km^{-1} (OME_{3-5}-fuel) compared to 209 g(CO_2-eq) km^{-1} (diesel fuel).[10] Deutz et al. investigated the WtW LCA for methylal (OME_1) and concluded that it has the potential to serve as an almost carbon-neutral blending component: replacing 24 wt.-% of diesel by OME_1 could reduce the GW impact by 22% and the emissions of NO_x and soot even by 43% and 75%, respectively.[28] However special sealing materials as EPDM[26,29] and fuel injection system modifications are needed after certain blending rates of OME with diesel fuel.[9] Neat OME applications are discussed using dedicated engines for niche markets (e.g. Agricultural engines, stationary engines, hand-used machinery, etc.) and for captive fleets (public buses, trains, etc.).[30,31]

Moreover, a recent study by Frontier Economics[32] concluded that Power-to-X (PtX) fuelled internal combustion engine vehicles (ICEVs) possess advantages over battery electrical vehicles (BEVs) considering the complete value chain efficiency and including the renewable generators yield efficiency and the fluctuating nature of renewable electricity production. Since PtX synthetic fuels could be produced wherever there are high renewable energy (RE) resources penetration and the dense fuels could be easily imported to the utilization point; PtX fuels can be dropped-in into existing infrastructure offering an efficient, fast and reliable solution. Particularly, for transport modes that indeed require high dense fuels (aviation, ships, trucks, etc.) there are no feasible means to achieve de-fossilization targets without PtX fuels.

OME production processes are investigated intensively since the early work by DuPont in the middle of the 20th century for longer chain OME production.[33] Since the 1990's short chain OME were recognized as interesting diesel blend or substitute.[34] Intensive research efforts since then for engine testing on one hand, and for production process on the other hand took place led by Ford Motor Company and Eni SpA.[35,36] From the early beginning of the 21st century fundamental developments led by BASF and BP corporation established the production processes for OME on research and pilot scale. Most of the following contributions on the process side were led by Chinese research and industrial groups importantly the work from China Petroleum & Chemical corporation SINOPEC.[33,37] An overview of publications and patents as well as the research activities in Germany and worldwide considering OME are given in the review work by Hackbarth et al.[38] elaborating the intensity of research in that field. Currently, some OME plants are in operation or under construction as reported in China with production capacities of 10 - 400 kt/a mostly based on commercial fossil based feedstock OME_1 or methanol and para formaldehyde (pFA) or formalin.[38] Unfortunately, the product quality, the reproducibility, and the long-term production capacities of such plants - due to varying operational strategies - are not defined. Additionally, the complexity of these plants to achieve pure OME products, limits the scalability of such technologies to the desired large-scale which is needed in fuel context.

Considering the value chain starting from H_2 and CO_2 towards OME production or partially considering the OME production based on the feedstock methanol, several techno-economic assessments (TEA) and process simulations for different synthesis routes were pursued. The studies highlighted insights regarding the economic potential of OME production as well as hurdles regarding the demonstration and technology realization. Prominently, the work from Burger et al.[39], Schemme et al.[40], Bongartz et al.[41], Ouda et al.[42], and Held et al.[43] are contemplated. The underlying assumptions, considered process routes, scopes of the evaluation, modelling approaches and boundary conditions are heterogeneous among these contributions, which leads to different conclusions and complicates the comparison between different process routes. Additionally, a complete and detailed process description identifying material and energy integration concepts of the sub-processes in a complete process chain where engineering data and TEA data can be extracted is lacking. The purification of the highly non-ideal and reactive product mixture containing several heterogeneous azeotropes, complex vapor-liquid-liquid equilibria (VLLE), especially the separation of water and formaldehyde from the target OME product and challenges regarding solidification are cumbersome. This leads to simplification strategies and assumptions, particularly on the product purification side which in some cases lead to misleading results concerning OME product composition and purity. Additionally, material and energy balances can deviate significantly from experimental cases.

In the light of the previous discussion, the introduction of OME into the market requires a detailed comparison of material and energy integrated, efficient, economically feasible and a scalable industrial process routes for the production of OME with a certain chain length.

Objectives

As part of the project Sustainable Mobility through Synthetic Fuels (NAMOSYN), the most promising OME production process routes are evaluated using a standardized simulation methodology with the objective to obtain the design parameters for the first European large-scale OME production process.

In addition to the OME production process concepts, the validation of the employed models using numerous published experimental data will be described. Furthermore, based on the modelling results, the material and energy integrated process, energy efficiency, carbon footprint and the TRL of the investigated process routes will be introduced and discussed. Complementary,

View Article Online
DOI: 10.1039/D1SE01370C

the net production costs of OME will be presented along with a sensitivity analysis covering the cost impact for H_2 and CO_2 showing the potential for a sustainable OME_{3-5} production. Finally, the understandings of this work highlight the critical process components in the OME value chain for further R&D endeavours.

2. Theory and Background

For the synthesis of OME, methyl capping groups as methanol (H_3C-OH, MeOH), methylal (H_3C-O-$(CH_2O)_1$-CH_3, OME_1), or dimethyl ether (H_3C-O-CH_3, DME) need to react over acid catalysts with a source for formaldehyde groups such as formalin, paraformaldehyde (HO-$(CH_2O)_n$-H with n = 8-100, pFA), trioxane ($C_3H_6O_3$, TRI), or anhydrous formaldehyde (H_2C-O, FA). The reaction proceeds through an initiation, growth, and termination mechanism as described by Baranowski et al.[44], Schmitz et al.[45–48], Oestereich et al..[49] This leads to several simultaneous catalyzed and non-catalyzed reactions and the formation of undesired side-products such as poly-(oxymethylene) hemiformals (HF), poly-(oxymethylene) glycols (MG), water, and others as shown in Figure 1 and extended in the ESI. The unstable HF and MG formation was experimentally investigated and quantified using NMR techniques in a succession of fundamental research work mainly by the group of Hasse et al.[50–53] That introduced the concept of the "overall composition" and the "true composition". The "true composition" is not measurable using standard analytical techniques and represents all the reaction mixture components namely: MeOH, H_2O, FA, OME_{1-n}, HF_n, MG_n and possible side products. The "overall composition" represents the decomposition of HF and MG to its original reactants MeOH, H_2O and FA. That is a deciding aspect in process modelling and simulation especially considering reaction and separation process design.[45–48] Estimations of heating and cooling duties, power loads and sizes of unit operation depend on thermodynamic and physical properties like heat capacities, enthalpies of vaporization and vapor pressures to account for a real phase behaviour and phase equilibria. Therefore, these results are influenced significantly by the true or overall composition. Besides, components like OME, HF and MG are not included yet in commercial flowsheet simulation software. The thermodynamic properties of such intermediates are described in the original literature but the right property implementation and consideration in a process simulation requires fundamental knowhow about this reactive system. The work from Maurer, Hasse, Burger and Schmitz et al.[45–48,54] offers a concrete basis for the validation of the simulation models. Furthermore, the methodology of the implementation of these reaction and phase behaviour consideration along the whole flowsheet simulation was introduced by Bongartz et al.[41] employing tool boxes from the electrochemical field namely the chemistry section in ASPEN plus® and is further modified in this work. There have been several significant modelling and simulation efforts to describe this complex system behaviour, the work from Burger et al.[35], Schmitz et al.[45–48], Bongartz et al.[41] and Ouda et al.[42] are duly acknowledged, and the simulation results generated in this work are a progression on that previous work.

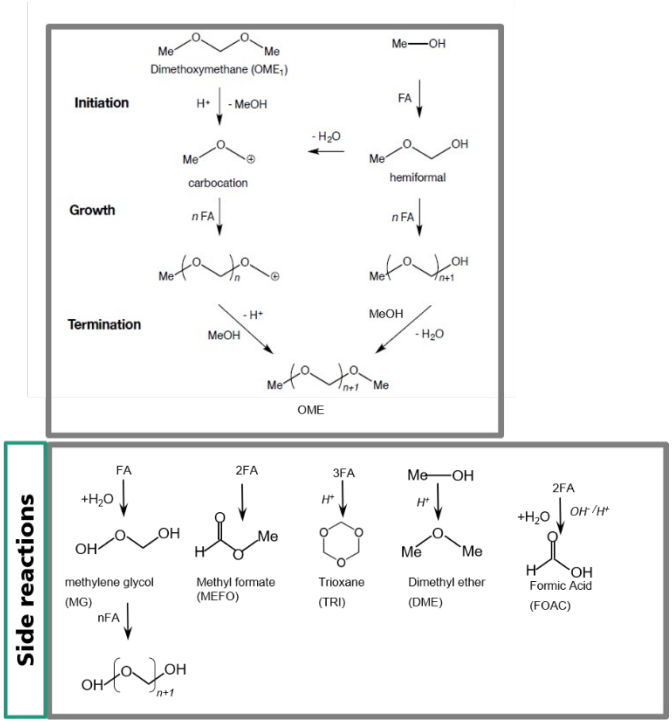

Figure 1 - Reaction network and mechanism of OME formation based on different methyl capping groups and formaldehyde, inspired by [44].

3. Process Description

As described previously OME can be produced starting from different feedstocks. Based on that, several process routes can be allocated to produce a desired mixture of OME_{3-5}. An overview of the four selected promising process routes investigated in this work is shown in Figure 2. The selection of the processes focused on the feedstock availability on large-scale, the technological maturity of the considered processes and the experimental data availability for consistent process evaluation.

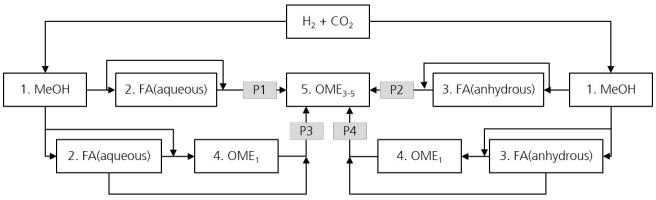

Figure 2 - Evaluated processes towards OME_{3-5}.

All four process routes in focus (denoted here P1-P4) start with the synthesis and the purification of MeOH from the feedstocks H_2 and CO_2. MeOH is converted into intermediate products namely FA and OME_1 which are further used to synthesize a mixture containing OME_n with n=1-10. This mixture is then fractionated to reach a final product mixture containing OME_{3-5}. Consequently, the conversion of MeOH to OME_{3-5} goes through different sub-processes, which in turn influences the total process energy efficiency and the product yields. These sub-processes are MeOH synthesis, FA(aqueous) synthesis, FA(anhydrous) synthesis, OME_1 synthesis and OME_n synthesis. The combinations thereof lead to the aforementioned production routes of OME. In the following section each of these sub-processes are briefly explained.

View Article Online
DOI: 10.1039/D1SE01270C

MeOH synthesis

MeOH synthesis is one of the oldest thermochemical processes with the highest production capacities and mainly is based on fossil feedstocks. The development of a Cu-based process enabled significant reduction of the synthesis conditions to temperatures as low as 200 - 280 °C and pressures 50 - 125 bar. Advanced catalyst development allows MeOH synthesis based on CO_2 rich feed with enhancing the catalyst water tolerance.[55,56] The process conditions for the MeOH synthesis are based on the work by Otto[57] and Bongartz et al..[58] The reaction network considered in this work is introduced in eq. 1-3. The reaction equilibrium and kinetic relations are implemented based on the work from Nestler et al..[59] The MeOH synthesis process takes place at 250 °C and 70 bar in a plug flow reactor and the downstream purification of MeOH from non-reacted gases such as CO_2, CO, H_2 and H_2O go through a cascade of flash drums with intermediate cooling operating at different pressure levels then followed by a distillation column. The light gases with the non-reactants are recycled back to the reactor to increase the product yield. A simplified flowsheet of this sub-process is included in Figure 3.

Main reaction network:

$$CO_2 + 3\ H_2 \rightleftharpoons CH_3OH + H_2O \quad (1)$$
$$CO + H_2O \rightleftharpoons CO_2 + H_2 \quad (2)$$
$$CO + 2\ H_2 \rightleftharpoons CH_3OH \quad (3)$$

FA (aqueous) synthesis

The FA(aqueous) sub-process comprises the conversion of MeOH to FA. Formalin or pFA are synthesized commercially from MeOH. The former is produced either via the silver catalyst-based process or the FORMOX process. In these processes, MeOH is partially oxidized over Ag-based catalyst or metal oxide-based catalyst to produce selectively formalin aqueous solution (FA concentration 37-55 m/m%). In the Ag-based process, MeOH is mixed with an air stream and fed to a reactor to be converted to FA via partial oxidation and dehydrogenation reactions as shown in eq. 4-6.
Main reaction network:

$$CH_3OH + ½\ O_2 \rightarrow CH_2O + H_2O \quad (4)$$
$$CH_3OH \rightleftharpoons CO + 2\ H_2 \quad (5)$$
$$CO + ½\ O_2 \rightleftharpoons CO_2 \quad (6)$$

FA(aqueous) synthesis sub-process takes place at T> 650 °C and near ambient pressure in a kinetically controlled regime. H_2O is formed as a by-product, for this reason this sub-process is denoted heron as FA(aqueous). The process concept of this sub-process was presented by Franz et al.[60], which considers the separation of FA from volatile gases in an absorber column using H_2O as a washing liquid. Providing a FA product stream containing about 55 m/m% FA and 45 m/m% H_2O, this stream should be concentrated to be further used for the synthesis of longer chain OMEs. Therefore, this stream is fed to a cascade of two evaporators which split it into two output streams. The target product from this sub-process stream with about 85 m/m% of FA is further used for the synthesis of longer chain OMEs, on the other hand, the evaporator side product stream with about 10 m/m% of FA is partially used as a washing liquid for the aforementioned absorber column and partially leaves the sub-process as a wastewater stream.

FA (anhydrous) synthesis

However, there is no commercial anhydrous FA synthesis based on the endothermic MeOH dissociation to monomeric FA and valuable H_2 (eq. 7), this route was investigated since 1960 to identify selective catalysts for the anhydrous FA synthesis.[61] The lack of direct application of the highly reactive monomeric FA product hinders the market establishment of this production route. In the case of OME synthesis, this valuable monomeric FA product is important, and this route is considered the “dream reaction”. The reaction occurs at high temperatures >650 °C which requires 85 kJ/mol FA produced. Due to the high reactivity of FA, the retention time is very short to avoid the formation of the thermodynamically unfavoured CO as shown in eq. 8. The challenge in this reaction system is to reach high MeOH conversions at high FA selectivity without deactivating the catalysts in this strongly reductive H_2 environment; an aspect that is intensively experimentally investigated in the scientific community. For the implementation in the simulation platform, the process described by Sauer et al.[62] combined with the process concept published by Ouda et al.[42] is adapted. MeOH is saturated in a carrier gas and further dissociated at 900 °C to FA and H_2 over a Na-based catalyst, following the conversion and selectivity experimentally investigated by Sauer et al..[62] CO is formed as an undesired side-product. For the separation of the monomeric FA from the reaction products, absorber columns using mainly MeOH or recycled OME fractions as washing liquids are used.
Main reaction network:

$$CH_3OH \rightleftharpoons CH_2O + H_2 \quad (7)$$
$$CH_3OH \rightleftharpoons CO + 2\ H_2 \quad (8)$$

OME_1 synthesis

Methylal is available commercially based on MeOH and FA feedstock. The OME_1 sub-process comprises the conversion of MeOH and FA to OME_1. For the sub-process implementation, the process concept was adapted from Drunsel.[63] The synthesis takes place in a heterogenous catalytic reaction at 60 °C and 2 bar over an acidic catalyst, e.g. Amberlyst® 15, in a plug flow reactor. Several reactions are possible as shown in the reaction network eq. 9-13. The reaction product purification takes place in a downstream reactive distillation column. The column is used to overcome the reaction equilibrium restrictions and to convert the rest of FA almost completely to OME_1, while separating H_2O and MeOH from the azeotropic mixture of OME_1 and MeOH. In a consecutive distillation column operating at a higher-pressure level, OME_1 is separated from the azeotropic mixture of OME_1 and MeOH and leaves the distillation column as the bottom product. The distillate product is recycled to the reactive distillation column.
Main reaction network:

$$CH_2O + H_2O \rightleftharpoons HO(CH_2O)_1H \quad (9)$$
$$CH_2O + HO(CH_2O)_{n-1}H \rightleftharpoons HO(CH_2O)_nH;\ n \geq 2 \quad (10)$$
$$CH_2O + CH_3OH \rightleftharpoons HO(CH_2O)_1CH_3 \quad (11)$$
$$CH_2O + HO(CH_2O)_{n-1}CH_3 \rightleftharpoons HO(CH_2O)_nCH_3;\ n \geq 2 \quad (12)$$
$$HO(CH_2O)_1CH_3 + CH_3OH \overset{H^+}{\rightleftharpoons} CH_3O(CH_2O)_1CH_3 + H_2O \quad (13)$$

Higher OME synthesis and purification

For the implementation in the simulation platform, the higher OME sub-process comprises the conversion of the aforementioned intermediates selectively to longer-chain OME and the purification of the target $OME_{3\text{-}5}$ product. The process concept adapted here is suitable for different feedstocks and was proposed by Schmitz et al..[39,46] OME_n synthesis takes place in a heterogenous

View Article Online
DOI: 10.1039/D1SE01270C

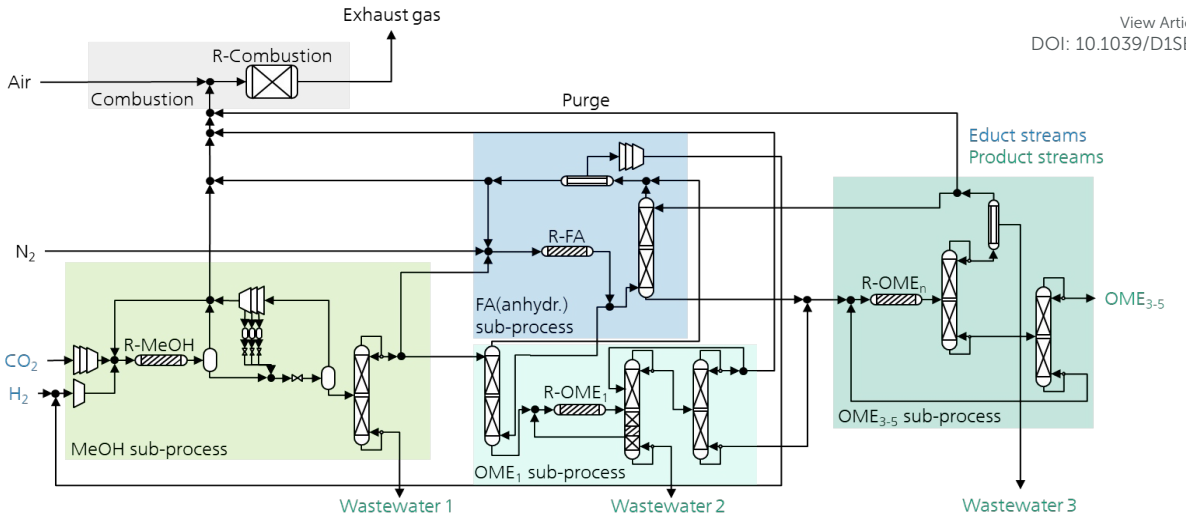

Figure 3 - Simplified process flow diagram for P4 allocation illustrating some material integration strategies and four of the five sub-processes discussed.

catalytic reaction at 80 °C and 2 bar in a plug flow reactor in presence of an acidic catalyst, e.g. Amberlyst® 46. The reaction network taking place here is presented in eq. 9-15 and summarized in Figure 1. The reaction product purification takes place in a cascade of two distillation columns and a membrane unit for the selective separation of H_2O after the first column as shown in Figure 3. The main product stream containing OME_{3-5} exits the sub-process and the streams containing $OME_{<3}$ and $OME_{>5}$ are recycled to the synthesis reactor.

Main reaction network:

$$HO(CH_2O)_nCH_3 + CH_3OH \overset{H^+}{\rightleftharpoons} CH_3O(CH_2O)_nCH_3 + H_2O;\ n \geq 2 \quad (14)$$

$$CH_2O + CH_3O(CH_2O)_{n-1}CH_3 \overset{H^+}{\rightleftharpoons} CH_3O(CH_2O)_nCH_3;\ n \geq 2 \quad (15)$$

Combustion

A combustion sub-process was implemented to use the energy of the purge streams to produce steam which was utilized in the sub-processes. For the simulation of the combustion reactions an adiabatic Gibbs reactor was applied, and excess air was added accordingly to achieve complete combustion and keep the adiabatic temperature rise below 800 °C. The stochiometric amount of O_2 required for a complete combustion can be estimated using eq. 16.

Main reaction network:

$$C_xH_yO_z + n\ O_2 + \rightarrow x\ CO_2 + 0.5y\ H_2O \quad (16)$$

Total process routes P1-P4

The combinations thereof lead to the production routes P1-P4 of OME. In the following section each of these total processes are briefly explained.

Process route **P1** constitutes of the sub-processes MeOH synthesis from H_2 and CO_2, FA(aqueous) synthesis and the combination of MeOH and aqueous FA to higher OME synthesis and purification.

Process route **P2** constitutes of the sub-processes MeOH synthesis from H_2 and CO_2 and FA(anhydrous) synthesis in which H_2 is produced as a by-product and separated and recycled to the MeOH sub-process. Downstream MeOH and anhydrous FA are synthesized to higher OMEs and purified. Almost no H_2O enters the OME_{3-5} sub-process, which reduces the formation of side-products and improves the process energy efficiency associated with smaller recycle streams. However, H_2O is still formed as a by-product in the synthesis of longer chain OMEs and needs to be separated out of the recycle stream using the membrane unit.

Process route **P3** constitutes of the sub-processes MeOH synthesis from H_2 and CO_2, FA(aqueous) synthesis and the combination of MeOH and aqueous FA to the OME_1 synthesis. OME_1 is further introduced with aqueous FA to the higher OME synthesis and purification. The advantage of P3 is the conversion of MeOH towards OME_1 prior to the synthesis of longer chain OMEs, which allows the separation of a large portion of the H_2O formed before the OME_n synthesis sub-process. In addition, fewer side-products are formed during the synthesis of longer chain OMEs, thereby reducing the energy demand during product purification towards OME_{3-5} and consequently enhancing the process energy efficiency.

Process route **P4** constitutes of the sub-processes MeOH synthesis from H_2 and CO_2, FA(anhydrous) synthesis and the combination of MeOH and anhydrous FA to the OME_1 synthesis. OME_1 is further introduce with anhydrous FA to the higher OME synthesis and purification. Hence, this affords the synthesis of longer chain OMEs from H_2O free reactants. This leads to no formation of the side-product H_2O and thus various other side-products are not formed. A very important advantage for the purification of the OME_n reaction product. This is very advantageous since the recycle of the H_2 side-product of the FA(anhydrous) synthesis leads to significant material and process energy efficiency improvements, in addition to the process energy efficiency improvement potential due to significantly less purification energy demand in the OME_{3-5} sub-process. More details on the process routes P1 to P4 are presented in the ESI.

4. Methodology

This chapter addresses general assumptions and system boundaries as well as the methodology of process modelling and simulation,

View Article Online
DOI: 10.1039/D1SE01270G

followed by process techno-economic and carbon footprint evaluation methodologies. Followed by the description of the comparison criteria.

General assumptions and system boundaries

The system boundaries were set for the evaluation on the simulation level from the feedstock H_2 and CO_2, followed by the synthesis of intermediates up to the desired product OME_{3-5}. It is assumed that the production plant is integrated in a chemical park where the necessary infrastructure for the provision of utilities such as steam, cooling water, etc. is available at market prices. CO_2 and H_2 are purchased as waste products or raw materials from renewable non-fossil sources. Waste streams of the processes are wastewater and exhaust gases. The wastewater is treated at market prices, while the waste gases are assumed to be released without further treatment. The OME_{3-5} production consists of several sub-processes, which are altogether material, and heat integrated. The obtained distribution of OME chain lengths in the final product OME_{3-5} differs slightly between the investigated routes. Nevertheless, it is assumed that in all cases the specification range is fulfilled without further processing and that the heating value from Held et. al.[43] represents the actual heating value in a good approximation. System boundaries are shown in Figure 4, further details on the assumptions are given in the ESI.

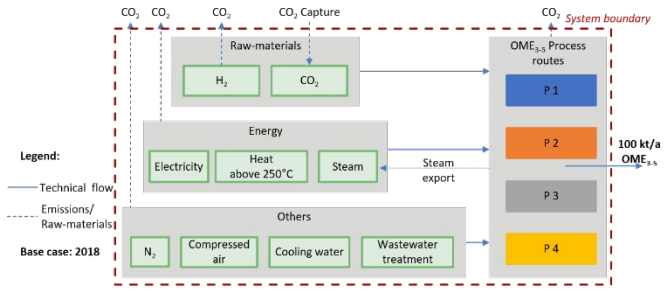

Figure 4 – System boundaries set on the simulation level of the process routes P1-P4.

Process modelling and simulation

Steady state simulations for P1 to P4 were implemented using Aspen Plus® software V11 from Aspen Technology Inc.. Aspen Energy Analyzer V11 and Aspen Process Economic Analyzer V11 were used for heat integration and unit operations dimensioning.

The components considered in the simulations are H_2, CO_2, CO, N_2, O_2, FA, MeOH, H_2O, OME_{1-10}, HF_{1-10} and MG_{1-10}. Most of these components as the acetals, glycols and OME are not included in a standard Aspen database, thus new components were added in the property analysis environment. An overview of the pure component thermodynamic and thermophysical properties used in the simulations can be found in the ESI.

To simulate purification processes, in particular thermal separations, interaction parameters are required which describe the real behaviour of the gas and the liquid phases. For mixtures that contain FA, a UNIFAC based model was introduced by Maurer et al..[54] This model was extended throughout the following decades by adding new components and by adapting the interaction parameters to new experimental data. Schmitz et al.[47] published a new version of the model considering OME_n which was adapted and implemented. An overview of the model and its validation is presented in the ESI. Adequate model parameter and implementation of the thermodynamic model is crucial for a realistic simulation of this special reactive mixture. A variety of reaction models describing the MeOH, FA(aqueous), FA(anhydrous), OME_1 and OME_n syntheses were used to assess the product compositions exiting the reactors. The models implemented in the simulation environment can be found in the process description of the sub-processes. The synthesis of FA was described based on conversion and yields from literature values, while the other syntheses were described according to published kinetic models. An overview of the employed reaction models is presented in the ESI.

Initially, the sub-processes were implemented separately in the simulation platform. Afterwards the material integration interconnecting these sub-processes together to describe process routes P1 to P4 was implemented. The production capacity was adjusted to 100 kt OME_{3-5} per year, and the heat integration was conducted to improve the overall process energy efficiency. Consequently, heat exchanger network was designed. After the network design, heat exchangers were interconnected in the process simulation to transfer heat from hot streams to cold streams and steam utilities were implemented to consider the steam supply by single process unit operations and the steam demand of other process unit operations. Subsequently, the process components were dimensioned. Based on the simulation material and heat balance, the utilities demand and main operational cost parameters were extracted. Since a complete process route is a combination of several sub-processes, more recycle loops which are interconnected should be converged. Standard numerical solvers in Aspen Plus® were used, while the complex loop convergence of the total process routes was achieved stepwise starting with connecting the sub-processes. After the material integrated loop convergence, heat integration of the total process routes was performed stepwise and followed by convergence of the energy integrated loop. The equipment sizing of unit operations followed the convergence and integration steps using Aspen Process Economic Analyzer V11. For these categorized as non-conventional unit operations namely: the membranes, heat exchangers, reactors, and the column dimensions for the FA(anhydrous) absorption considered as ideal separation units, literature-based sizing methods were adapted. Membrane areas were evaluated according to the methods described in Schmitz et al.[47] and Baker.[64], while the column dimensions were estimated correlating to the absorption column in the aqueous FA sub-process. A detailed description of the procedure for dimensioning the process components and the heat integration procedure applied for the process routes can be found in the ESI.

Process evaluation and comparison criteria

The implemented processes P1 to P4 were evaluated using various key performance indicators (KPIs). These KPIs were translated into process evaluation criteria used to compare the process routes, since they provide a concise summary of the different process routes in terms of mass and energy balances. The process routes utility demands and process energy efficiencies were evaluated based on the total mass and energy balances from P1 to P4.

In this work the energy efficiency of the overall process η_{Energy} is defined in eq. (17).

$$\eta_{Energy} = \frac{\dot{m}_{OME_{3-5}} \cdot LHV_{OME_{3-5}}}{\sum_k \dot{Q}_k + \sum_l \dot{W}_l + \sum_i \dot{m}_i \cdot LHV_i} \quad (17)$$

where $\dot{m}$ denotes the mass flow rate of reactants i and the OME_{3-5} containing product stream. LHV is the lower heating value at 298 K, while $\dot{Q}_k$ and $\dot{W}_l$ represent externally supplied heat fluxes and electric power demand, respectively.

In addition to the energy efficiency of the process routes, an assessment of the material balance was made, and the performance was indicated by two parameters. The first parameter η_C reflecting the carbon efficiency, i.e. the ratio of carbon atoms C in the feedstock and the carbon atoms in the OME_{3-5} product stream, as defined in eq. (18). The second parameter η_{Mass} considers the mass flow rates, i.e. the ratio of the OME_{3-5} product mass flow rate with respect to the feedstock mass flow rate, as defined in eq. (19).

$$\eta_C = \frac{C_{OME_{3-5}}}{\sum_i C_i} \quad (18)$$

$$\eta_{Mass} = \frac{\dot{m}_{OME_{3-5}}}{\sum_i \dot{m}_i} \quad (19)$$

where $\dot{m}$ denotes the mass flow rate of the reactants i.

Economic evaluation

The methodological approach for production cost estimation is a factorial method described by Peters et al.[65] on the basis of the equipment data and material and energy streams obtained from the process simulations. The calculations are carried out with the DLR-inhouse software techno-economic process evaluation tool (TEPET) in an automated and standardized manner.[66]

The targeted parameters of the economic analysis are the investment and operating costs as well as the net production costs related to a production unit. An overview of the most important assumptions for the economic evaluation is given in Table 1 (detailed list is given in the ESI).

The net production costs of fuels from renewable H_2 and CO_2 are typically highly sensitive on the raw material price of the educts.[67] Hence, the future price development exhibits a high uncertainty. Consequently, a wide range of CO_2 and H_2 costs was examined evaluating the influence of cost variations.

Table 1: General assumptions for the economic analysis.

Description	Value	Reference
Base year	2018	
Annual full load hours	8000 h/a	
Plant operation time	20 a	
Plant capacity	100 kt/a	
Place of location	Germany, chemical park	
CO_2 cost, base case	309 €/t_{CO2}	[68]
CO_2 cost, variation range	65 to 700 €/t_{CO2}	Lower limit:[69] Higher limit:[70]
H_2 cost, base case	4241 €/t_{H2}	[68]
H_2 cost, variation range	1500 to 6600 €/t_{H2}	[71]
LHV_{H_2}	33.3 kWh/kg_{OME3-5}	[43]
$LHV_{OME_{3-5}}$	5.25 kWh/$kg_{OME_{3-5}}$	[43]
LHV_{diesel}	11.9 MJ/kg_{diesel}	[72]

Capital expenditures (CAPEX)

CAPEX are calculated on the basis of purchased equipment costs of the main process equipment. The equipment were categorized as conventional and non-conventional and the sizing data were obtained based on the simulation results explained in the previous section and is further explained in the ESI.

For conventional unit operations: packed columns and shell-and-tube heat exchangers were assumed as equipment types for all applied columns and heat exchangers, respectively. For H_2 compression reciprocating compressors were assumed, while all other compressors were taken as centrifugal-rotary ones. Knock-out drums were considered as storage vessels for the cost calculation.[73] The costs of multistage compressor cooling, absorber cooling and column reboilers and condensers were considered applying shell-and-tube heat exchanger costs. Reflux pumps were considered separately in the column cost calculation while the costs for column insulation and connections were neglected. 316 stainless steel was assumed as standard material due to the presence of FA in the process,[74] except for the burner consisting of carbon steel. For non-conventional unit operations: For H_2O membranes plate-and-frame modules were assumed, while the membranes for H_2 separation were taken as hollow-fiber modules in accordance to Baker.[64]

The use of one uniform data basis was preferred in the selection of the specific cost for the different types of equipment. Hence, cost functions from Peters et al.[65] were applied if appropriate. Specific costs from other references than Peters et al.[65] were only chosen in the case of multitube reactors, fixed-bed reactors, thin film evaporators and membrane modules due to inadequate capacity ranges or the lack of data given in Peters et. al..[65] A detailed explanation for the deviations from the standard reference and the related assumptions is given in the ESI. When the capacity limit of the chosen cost function was exceeded, the equipment was separated formally into the minimum number of equally sized components to fit the given range.

Lang factors for fluid processing plants are assumed for the calculation of the additional direct and indirect CAPEX from the purchased equipment cost.[65] Reduced Lang factors for main compressors were assumed considering a reduced share of additional CAPEX in the case of compressors larger than 1000 kW of nominal power. An overall cost factor of 2.27 (compared to 5.93 for all other equipment) was applied.[68] Fixed capital investment (FCI) is calculated from the total direct and indirect cost by assuming an additional share of contractor's fee and contingencies.[65] The total capital investment (TCI) includes a working capital of 15% of the TCI.[65] Annual capital cost (ACC) are determined from TCI by the annuity method[65] assuming an interest rate of 5%. More details of the methodological approach are described by Albrecht et al..[66] All applied Lang factors are given in the ESI.

Operational expenditures (OPEX)

For the determination of raw material and utility costs ($OPEX_{R\&U}$) all mass and energy input streams as well as wastewater output streams and surplus steam provided by the simulation results are considered.

View Article Online
DOI: 10.1039/D1SE01270C

H_2 and CO_2 costs in the base case were taken from generic values,[68] which were calculated following the same assumption basis as in this work. The lower limit of the considered CO_2 cost range was taken from Naims[69]. In this reference, CO_2 costs for carbon capture from various point sources are examined and a value of approx. 65 €/t_{CO2} is estimated for a large-scale carbon capture and utilization (CCU) scenario. For the upper limit, a value of 720 €/t_{CO_2} was applied according to House et. al.[70] for direct air capture (DAC). To the best of the authors' knowledge, this represents the highest CO_2 cost from DAC published to date.[75,76] H_2 cost ranges are taken from Hydrogen Europe report[71] considering steam methane reforming (SMR) costs as lower limit, which is assumed to be the target value for green H_2 costs that could possibly be reached by proposed optimization strategies. The conservative estimations of electrolysis cost from wind power is taken as the upper limit.[71] The assumed H_2 and CO_2 cost ranges are given in Table 1.

The demand of high temperature heat (>250°C) is covered by electrical power assuming a power-to-heat efficiency of 95% for energy conversion.[77] All catalysts are considered as raw material streams calculated from the catalyst lifetime. The costs are estimated from the trading price in the case of silver and by extrapolation of low quantity prices on bulk prices in the case of all other catalysts. All other specific costs for raw material and utilities as well as the assumed catalyst lifetimes are given in the ESI.

Employee-hours per year (h_{labor}) are estimated from the characteristic plant capacity and the number of production steps according to the procedure proposed by Peters et al..[65] Specific labor costs for Germany are assumed.[78] Additional direct and indirect operational expenditures ($OPEX_{dir/ind}$) are calculated with the factorial method described in Peters et. al.[65] and Albrecht et. al..[66] As only the manufacturing costs are determined, no costs for distribution and selling as well research and development are considered. All applied cost factors are given in the ESI.

Net production costs (NPC)

Specific net production costs (NPC) are calculated from ACC, total OPEX and the product output and related to a litre diesel equivalent (l_{DE}) according to:

$$\mathrm{NPC} = \frac{\mathrm{ACC} + \mathrm{OPEX_{dir}} + \mathrm{OPEX_{ind}} + \mathrm{OPEX_{R\&U}} + h_{labor} c_{labor}}{\dot{m}_{OME_{3\text{-}5}} \frac{LHV_{OME_{3\text{-}5}}}{LHV_{diesel}\, \rho_{diesel}}} \quad (20)$$

$$= \mathrm{ACC'} + \mathrm{OPEX'_{dir}} + \mathrm{OPEX'_{ind}} + \mathrm{OPEX'_{R\&U}} + C'_{labor}$$

with the output $OME_{3\text{-}5}$ mass flow $\dot{m}_{OME_{3\text{-}5}}$, the lower heating value $LHV_{OME_{3\text{-}5}}$ of $OME_{3\text{-}5}$,[43] and the lower heating value LHV_{diesel} and density ρ_{diesel} of diesel.[72]

CO_2 footprint evaluation

LCA is a methodology for evaluating the environmental impacts of product systems along the entire life cycle. LCA is standardized in the ISO 14040/14044 standards[79,80] and considers all environmental impacts of material and energy flows that are exchanged with the environment.

The carbon footprints of the four process routes P1-P4 for $OME_{3\text{-}5}$ are compared by applying a well-to-tank approach. The system boundaries of all routes with feedstock and energy supply are described above and shown in Figure 4. Note that the CO_2 emissions from use-phase and end-of-life phase of $OME_{3\text{-}5}$ is neglected since both are identical for all four routes and thus neutralize each other in a comparison. The construction of chemical plants is neglected in this analysis due to lack of data.

Comparing technologies consistently requires a common basis. In LCA, this common basis is the so-called „functional" unit.[77] For the well-to-tank approach, we choose as functional unit "the provision of 1 MJ of enthalpy of combustion" and additionally present the results per litre diesel equivalent. For this study, we focus on evaluating the carbon footprint in the life cycle impact assessment (LCIA) of the four alternative process routes. The environmental impacts are assessed in accordance to the LCIA methodology "ReCiPe Midpoint (H) V1.13 no long-term (LT)" following the methodological guidelines for LCA of synthetic fuels of the research center for energy economics (FfE).[81] Although other impact categories are also relevant, they are beyond the scope of this study.

For the life cycle inventory (LCI), we consider generic process data of the FfE for H_2, CO_2, and electricity supply as shown in Table 2.[68] For the electricity supply, we consider today's electricity grid mix in Germany as it is modelled in the guideline of FfE. For process heat, we assume that heat below 250 °C is supplied by steam that is produced as energy carrier in the chemical industry[82], while for heat above 250 °C we assume an electrode boiler with a Power-to-Heat efficiency of 95 %.[77] Note that the processes routes P1, P2, and P4 export steam, for which we consider an environmental credit, i.e., avoided burden, for steam production as energy carrier in the chemical industry.[82] For the H_2 supply, we consider the average carbon footprints of an alkaline electrolysis (AEL), solid oxide electrolyser cell (SOEC), and a polymer electrolyte membrane (PEM) electrolysis. Note though that conventional SMR would result in a lower carbon footprint of H_2 supply than an electrolysis combined with today's electricity grid mix in Germany: The carbon footprint of today's German electricity grid mix, as it is considered in our base case year 2018, is considerably high with 24.93 kg CO_2-eq./kg H_2. For this reason, we analyze the influence of electricity supply on the carbon footprint in a sensitivity analysis in Figure 13. CO_2 is supplied by the average of DAC and mono-ethanol amine (MEA) scrubbing in the cement industry. The environmental credit, i.e., avoided burden, for CO_2 utilization is credited to the $OME_{3\text{-}5}$ production.

For additional process data for the supply of utilities like nitrogen, compressed air, cooling water, and wastewater treatment, we consider LCA datasets of the ecoinvent database.[82] See the ESI for more details on the used LCA datasets.

Table 2: General assumptions for the LCA datasets of H_2, CO_2, and electricity supply in the base case year 2018 in accordance with the guideline of FfE.[81]

Description	Value	Reference
H_2 supply	24.93 kg CO_2-eq./kg H_2	81
CO_2 supply	-0.76 kg CO_2-eq./kg CO_2	81
Electricity supply	0.50 kg CO_2-eq./kWh_{el}	81

View Article Online
DOI: 10.1039/D1SE01370A

Technology Readiness Level (TRL)

TRL is defined as a criterion for evaluating the development status of new technologies based on a systematic analysis and indicates on a scale of 1 to 9 how advanced a technology is. The TRL of the five individual sub-processes and the total process routes P1-P4 were assessed on the basis of the published TRL scale in the energy research program of the German Federal Government addressing the innovations for the energy sector.[83] The TRL scale is presented in the ESI.

For the purposes of assigning the TRL of the total process routes P1-P4, it was not only the sub-process with the least TRL that we considered to determine the TRL of the total process route, rather we also assigned a mean TRL value for the sub-processes. Thereby, a better comparison of the TRL of the total process routes is possible. Since all process routes are limited by individual process components such as the FA synthesis reactor in the FA (anhydrous) sub-process and the H_2O separation unit in the $OME_{3\text{-}5}$ sub-process. Limiting the TRL of the total process routes to the aforementioned process components would reduce the TRL of P1 to P4 to TRL 3-4 while P1 and P3 in fact would benefit from the high TRL of the FA(aqueous) sub-process. For this reason, the mean TRL value allows for a realistic presentation of the significant research and development work which remains to be done to realize the process routes to any considerable extent.

5. Results and discussion

Process simulation and evaluation

Energy and Mass balance

After implementing the complete processes in the simulation platform and applying the described methodologies, the results were used for evaluation and comparison. In Figure 5 a summary of the results of the mass and energy balances of P1-P4 is shown in form of e-Sankey diagrams. In addition, the input and output streams are listed in Table 3 with respect to the main product stream $OME_{3\text{-}5}$, accounting for the results of the mass balances at a production of 100 kt/a $OME_{3\text{-}5}$.

Table 3: Results of the mass balance for P1 to P4 for a production of 100 kt/a $OME_{3\text{-}5}$.

	P1	P2	P3	P4
Total Input [$kg/kg_{OME3\text{-}5}$]	7.54	8.19	7.58	8.53
H_2	0.27	0.21	0.27	0.21
CO_2	1.96	2.18	1.94	2.20
N_2	-	0.20	-	0.20
Air*	5.32	5.60	5.37	5.92
Total Output [$kg/kg_{OME3\text{-}5}$]	7.54	8.19	7.58	8.53
$OME_{3\text{-}5}$	1.00	1.00	1.00	1.00
OME_3	0.43	0.46	0.44	0.43
OME_4	0.38	0.35	0.36	0.36
OME_5	0.19	0.19	0.18	0.21
Wastewater	1.30	0.98	1.28	1.00
Exhaust gas	5.24	6.21	5.30	6.54

*Air used for the FA(aqueous) synthesis and for the combustion of purge streams while the generated heat was utilized in the processes as shown in Figure 3.

The mass balance evaluation of P1-P4 shows that P1 and P3 require more H_2 and less CO_2 feedstock in comparison to P2 and P4 to produce the targeted 100 kt/a $OME_{3\text{-}5}$. In fact, that is the outcome of the two different process design concepts for the FA production relying on aqueous or anhydrous FA. In addition, this results in a higher production of H_2O which is the by-product of the acetalization reaction and exits the process as wastewater streams in the case of P1 and P3. Moreover, P1 and P3 have smaller exhaust gas flows due to the use of O_2 as feedstock for the FA(aqueous) sub-process. In contrast, the FA(anhydrous) sub-process considered in P2 and P4 N_2 is used as a carrier for the feedstock MeOH which should be introduced at certain dilution to the FA reactor. As a result of purging out a portion of the carrier gas to prevent the accumulation of the side product CO, the FA(anhydrous) sub-process has a higher exhaust gas flow. In addition, the side product CO of the FA(anhydrous) sub-process leads to a higher demand of CO_2 for P2 and P4. On the other hand, the H_2 side product of the endothermic MeOH dissociation reaction in the anhydrous FA synthesis, lowers the demand for the total process H_2 feedstock in comparison to P1 and P3. Consequently, this results in higher input and output mass flows for P2 and P4. In addition, OME_3, OME_4 and OME_5 compositions reveal small differences between the process routes. The simulations, however, focused on similar product compositions rather than minimal recycle flows to define the feedstock composition of the $OME_{3\text{-}5}$ sub-process. This approach is based on the assumption that product composition is of greater importance to the application than the process energy efficiency of the production process.

In Table 4, the energy flows of the input and output streams are shown relative to the energy flow of the product stream $OME_{3\text{-}5}$ for P1-P4. The energy flow is expressed as the product of LHV and mass flow. In addition, the energy demand in terms of electricity, steam, cooling water and heat utilities above 250 °C is shown relative to the $OME_{3\text{-}5}$ product stream.

The energy balances of the considered process routes show that P2 and P4 require more electricity, mainly due to the higher energy demand at high temperature level >250 °C for the FA(anhydrous) synthesis. Additionally, the higher dilution rate required for the successful conversion of MeOH to FA and H_2 increases the demand for compression recycling the carrier gas stream.

Table 4: Results of the energy balance for P1 to P4 for a production of 100 kt/a $OME_{3\text{-}5}$.

	P1	P2	P3	P4
Total Input [$kWh_{LHV}/kWh_{OME3\text{-}5,\ LHV}$]				
H_2	1.70	1.33	1.69	1.34
Total Output [$kWh_{LHV}/kWh_{OME3\text{-}5,\ LHV}$]				
$OME_{3\text{-}5}$	1.00	1.00	1.00	1.00
Energy demand [$kWh/kWh_{OME3\text{-}5,\ LHV}$]				
Electricity	0.09	0.13	0.09	0.14
Steam, 4 bar	-0.10	-0.07	0.09	0.24
Steam, 20 bar	0.30	0.26	0.16	-0.07
Cooling water, 15-20 °C	-0.19	-	-0.19	-
Cooling water, 15-25 °C	-0.86	-0.91	-0.92	-0.79
Heat, T > 250 °C	-	0.19	-	0.19

View Article Online
DOI: 10.1039/D1SE01270C

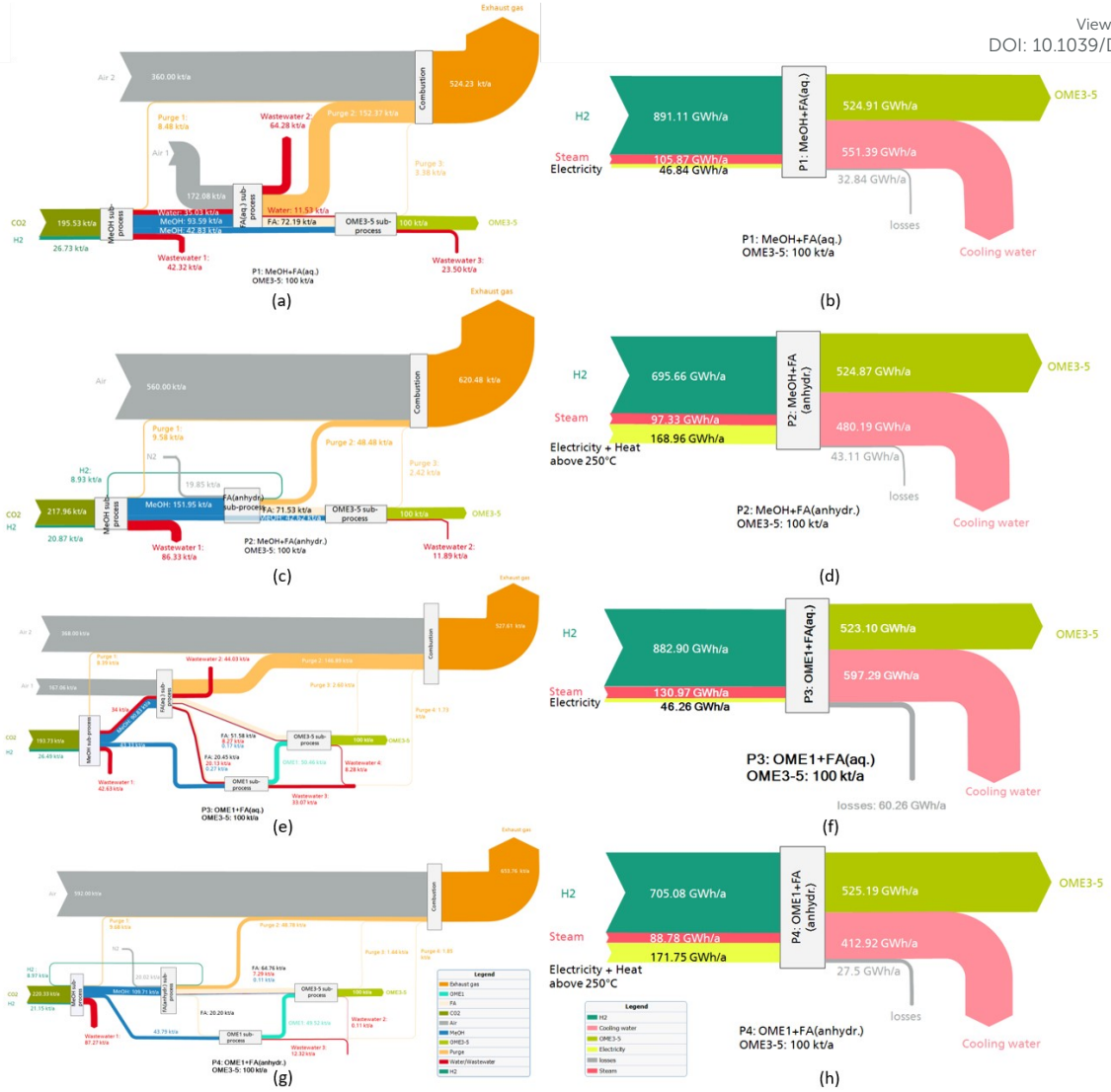

Figure 5 – e-Sankey diagrams for (a) mass balance of P1, (b) energy balance of P1, (c) mass balance of P2, (d) energy balance of P2, (e) mass balance of P3, (f) energy balance of P3, (g) mass balance of P4 and (h) energy balance of P4.

Moreover, P1, P2 and P4 show negative steam demands in the case of 4 or 20 bar, which is mainly due to the fact that the steam generated in the MeOH synthesis reactor is used to supply the heat to the reboilers in the OME_{3-5} sub-process. This effect was also elaborated by Schemme et. al..[40] In addition, different feedstocks for the OME_{3-5} sub-process result in different mass flows being fractionated in the distillation columns due to side-product formation, which in turn leads to different reboiler and condenser duties. The absorber of the FA(aqueous) sub-process requires cooling water with maximum temperature rise up to 20 °C. Overall, P1 and P3 show a lower electricity demand, a higher steam and cooling water demand but no demand for heat above 250°C.

Process efficiencies

Based on the methodology discussed in section 3, different process energy and material efficiencies were evaluated and the results are listed in Table 5 and presented in Figure 6.

Table 5: Results of the process efficiencies for P1 to P4 and literature results [40, 43, 41].

	P1	P2	P3	P4	Literature
η_{Energy} [%]	50.3	54.6	49.3	54.4	31-60
η_{C} [%]	81.6	73.2	82.1	72.5	
η_{Mass} [%]	38.1	41.9	38.5	41.4	

Process routes P2 and P4 comprising the anhydrous FA synthesis sub-process exhibit the highest energetic efficiencies due to the recycling of the valuable side product H_2 as a feedstock. In contrast, P2 and P4 exhibit lower carbon efficiencies principally due to the side reaction in the FA(anhydrous) synthesis to CO. Evidently, as shown in Table 4, the lower energetic efficiencies of P1 and P3 arise principally from the higher H_2 demand, which is not fully compensated for by the heat required at above 250 °C in P2 and P4. The lower overall material efficiency η_{Mass} of feedstock being converted to OME_{3-5} for P1 and P3 is a result of the production of large amounts of the side product H_2O in the FA(aqueous) synthesis due to MeOH the partial oxidation reaction. This generated H_2O is separated with large effort

View Article Online
DOI: 10.1039/D1SE01270C

downstream to the FA(aqueous) sub-process and leaves the process in form of wastewater.

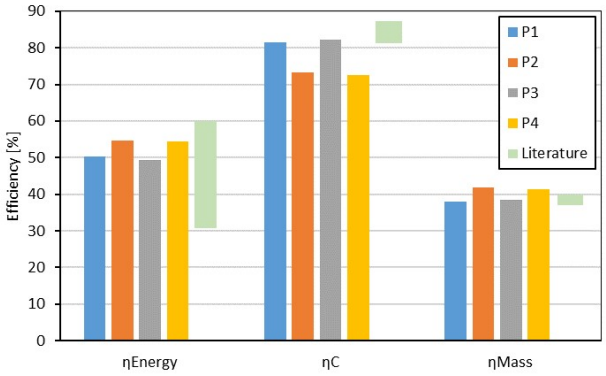

Figure 6 - Results of the process efficiencies for P1 to P4.

Held et al.[43] investigated different scenarios to produce OME_{3-5} based on stochiometric material balances together with different heat integration strategies within the sub-processes and carbon capture scenarios for the feedstock CO_2. Particularly, one scenario allows for heat integration between all sub-processes in combination with CO_2 from point sources (CPS) assuming CO_2 is available for zero incremental energy costs. This scenario is consistent with our CO_2 feedstock assumptions which consider purchasing already prepared CO_2 without extending the system boundaries to include the separation and preparation of CO_2. Under this scenario, a process energy efficiency of 59-60% was estimated, in fact slightly higher than the process energy efficiency estimated in this work. The difference is particularly a result of the different level of detail considered for the process simulation. Schemme et. al.[40] and Burre et. al.[41] also investigated different routes to produce OME_{3-5} based on H_2 feedstock. However, in these studies, a process energy efficiency of 31-40% was estimated, which is significantly lower than the values estimated in this work being rather close to the results from Held et. al.[43] scenario in which heat integration is only considered within the sub-processes themselves rather than within the entire process chain. Hence, this highlights the impact and importance of heat integration on process energy efficiency with respect to the entire process route. In other words, the effect of using the surplus heat from the MeOH sub-process throughout the entire process heat integration has a positive impact on the process energy efficiency.

Economic evaluation

CAPEX base case

An overview over the calculated CAPEX is given in Table 6. The obtained purchased equipment cost (EC) differs significantly ranging from 28 Mio€ in the case of P3 up to 49 Mio€ in the case of P2.

Table 6: Calculated CAPEX for process routes P1-P4

	P1	P2	P3	P4
EC [Mio€$_{2018}$]	29	49	28	40
FCI [Mio€$_{2018}$]	128	215	126	182
ACC [Mio€$_{2018}$/a]	11	19	11	16

The contribution of the different process steps and the different types of equipment to the overall equipment cost is shown in Figure 7. Main contributors are the MeOH and the FA (aqueous/anhydrous) sub-processes in all routes. With respect to the equipment type, compressors and heat exchangers exhibit generally the highest share of equipment costs. The marginal contribution of the pump costs amounts to less than 1% for all routes.

The elevated EC of route P2 and P4 result mainly from the FA(anhydrous) sub-process, while the EC of all other process steps only differ slightly between the different routes. Remarkably, the additional OME1 sub-process of route P3 and P4 does not lead to a significant increase in EC compared to the routes P1 and P2 without an OME_1 step. The high EC of the FA(anhydrous) sub-process can be explained by the elevated reaction temperature (900°C) compared to the FA(aqueous) sub-process (650°C) and the additional separation and recycle of H_2 to the MeOH sub-process involving compression from 2 to 29 bar. This leads to larger heat exchanger areas and a higher demand of compression work in comparison to the FA(aqueous) sub-process and therefore to higher costs for heat exchangers and compressors. A detailed breakdown of the calculated EC is given in the ESI.

In total, the calculated FCI ranges from around 130 Mio€, in the case of P1 and P3, to 215 Mio€ for P2 resulting in ACC between 11 Mio€/a and 19 Mio€/a.

OPEX base case

Table 7 gives an overview of the calculated OPEX. Main contributors to the overall operational costs are the $OPEX_{R\&U}$, while labor costs and other direct and indirect OPEX only contribute to around 10 % in total.

Table 7: Calculated OPEX for route P1-P4.

	P1	P2	P3	P4
$OPEX_{R\&U}$ [Mio€$_{2018}$/a]	194	177	193	179
Labor costs [Mio€$_{2018}$/a]	4.2	4.2	5.4	5.9
$OPEX_{dir}$ [Mio€$_{2018}$/a]	4.4	6.4	4.8	6.2
$OPEX_{ind}$ [Mio€$_{2018}$/a]	6.4	8.7	7.2	9.0
$OPEX_{tot}$ [Mio€$_{2018}$/a]	209	196	210	197

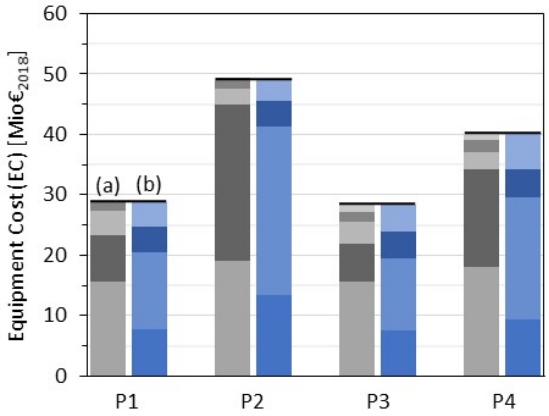

Figure 7 - Breakdown of the equipment costs of the routes P1-P4 (a) by synthesis steps, left grey column from bottom to top: MeOH, FA(aqueous or anhydrous), OME_{3-5}, heat recovery, OME_1 (only P3 and P4); (b) by equipment type, right blue column from bottom to top: compressors, heat exchangers, reactors, separators; The marginal contribution of pump costs is not visible in this diagram.

View Article Online
DOI: 10.1039/D1SE01270C

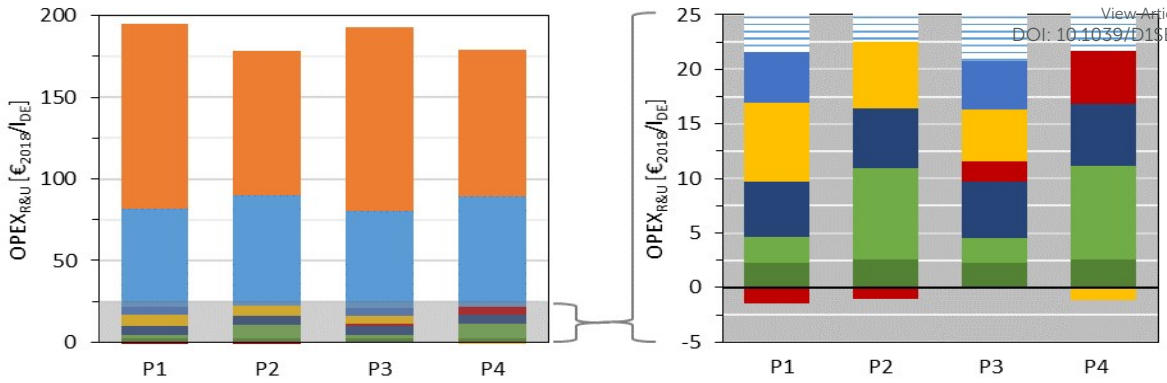

Figure 8 - Breakdown of raw material and utility R&U costs of the routes P1-P4: H_2, CO_2, silver (FA, aqueous), 20 bar steam, 4 bar steam, compressed air, electricity, remaining.

A breakdown of $OPEX_{R\&U}$ is shown in Figure . As expected, CO_2 and H_2 costs have by far the greatest impact on $OPEX_{R\&U}$. They range from 60 Mio€/a (P1/P3) to 68 Mio€/a (P4) for CO_2 and from 89 Mio€/a (P2) to 113 Mio€/a (P1) for H_2 in the base case. The lower H_2 costs in P2 and P4 compared to P1 and P3 result from the FA(anhydrous) sub-process, which allows higher H_2 efficiency since less or no H_2O is generated as a side product. However, the savings are diminished by the somewhat higher CO_2 demand in P2 and P4 due to the considerable amount of CO formed as by-product which leads to higher purge rates in the FA(anhydrous) synthesis.

The residual $OPEX_{R\&U}$ amount to around 15 Mio€/a for all routes. Main contributors are steam, compressed air, and electricity as well as the silver catalyst in the case of P1 and P3. It should be noted that silver catalysts can be regenerated electrolytically with negligible material and activity loss.[60,84] This may lead to a reduction of silver catalyst costs. However, due to the low overall impact the consideration of silver regeneration was beyond the scope of the present work. Selling of excess heat in P1, P2 and P4 which cannot be integrated into the processes only leads to minor revenues compared to the overall utility cost. A detailed breakdown of the calculated $OPEX_{R\&U}$ is given in the ESI.

NPC base case

A breakdown of the NPC is shown in Figure . The lower CAPEX of P1 and P3 are compensated by the somewhat higher raw material cost. In general, raw material costs have by far a higher impact on the NPC than CAPEX.

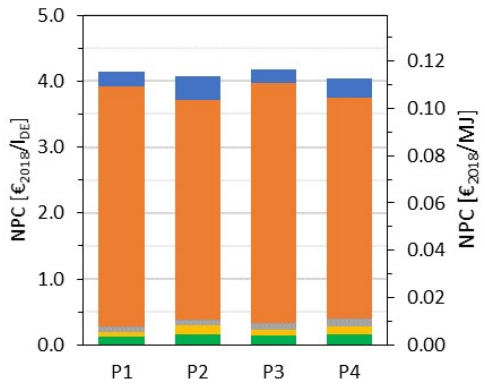

Figure 9 - Breakdown of net production costs (NPC) of the routes P1-P4: ACC′, $OPEX'_{R\&U}$, C'_{labor}, $OPEX'_{dir}$, $OPEX'_{ind}$.

The calculated NPC amount to 4.14 €$_{2018}$/l$_{DE}$ for P1, 4.05 €$_{2018}$/l$_{DE}$ for P2, 4.18 €$_{2018}$/l$_{DE}$ for P3 and 4.05 €$_{2018}$/l$_{DE}$ for P4. However, it has to be pointed out that the deviations are small in consideration of the uncertainty of the net production cost estimation.[66]

Variation of CO_2 and H_2 price

NPC were calculated for a wide range of CO_2 and H_2 costs to examine the influence of the variability of future price developments. The results are shown in Figure 10 and Figure 11 for the variation of the CO_2 and H_2 cost, respectively, fixing the other raw material cost on the base case. This is extended in Figure 11 (right) where H_2 cost is varied against different CO_2 cost scenarios covering a wide range of production locations worldwide and business cases. The high dependency of the NPC on the CO_2 and H_2 price is illustrated. In the case of CO_2 cost variation, NPC between 3.0 €/l$_{DE}$ and 5.8 €/l$_{DE}$ are obtained, while the variation of the H_2 price leads to 2.8 to 5.4 €/l$_{DE}$ of NPC. The maximum discrepancy between the different routes is observed at the lower limit of the CO_2 cost range between P3 (3.3 €/l$_{DE}$) and P4 (3.0 €/l$_{DE}$) and at the higher limit of the H_2 cost range between P2/P4 (5.0 €/l$_{DE}$) and P3 (5.4 €/l$_{DE}$). However, these discrepancies of maximum 10% are still small in consideration of the uncertainty. Additionally, Figure 11 (right) represents P4 for the variation of the CO_2 cost with the variable H_2 cost. Hence, the NPC ranges from 1.7 €/l$_{DE}$ and 6.7 €/l$_{DE}$. Whereas the dashed green line represents the highest NPC of P4 with variable H_2 cost and a DAC price of 720 €/t$_{CO_2}$,[70] the price range for carbon capture with DAC technology is currently subject to great uncertainties, ranging from 100 to 800 €/t$_{CO_2}$.[85]

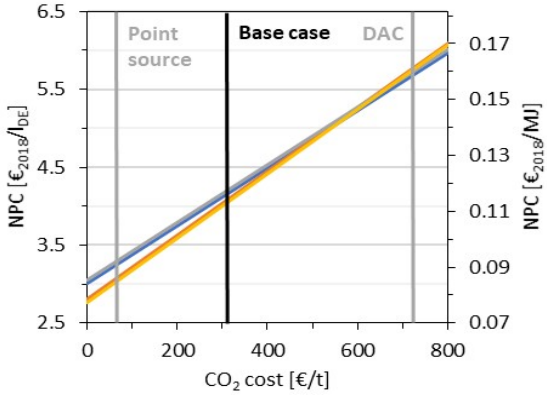

Figure 10 - Dependence of NPC on the CO_2 cost: P1, P2, P3 P4; Point source cost from[69], DAC cost from[70]; All other raw material costs are fixed on the base case.

View Article Online
DOI: 10.1039/D1SE01270C

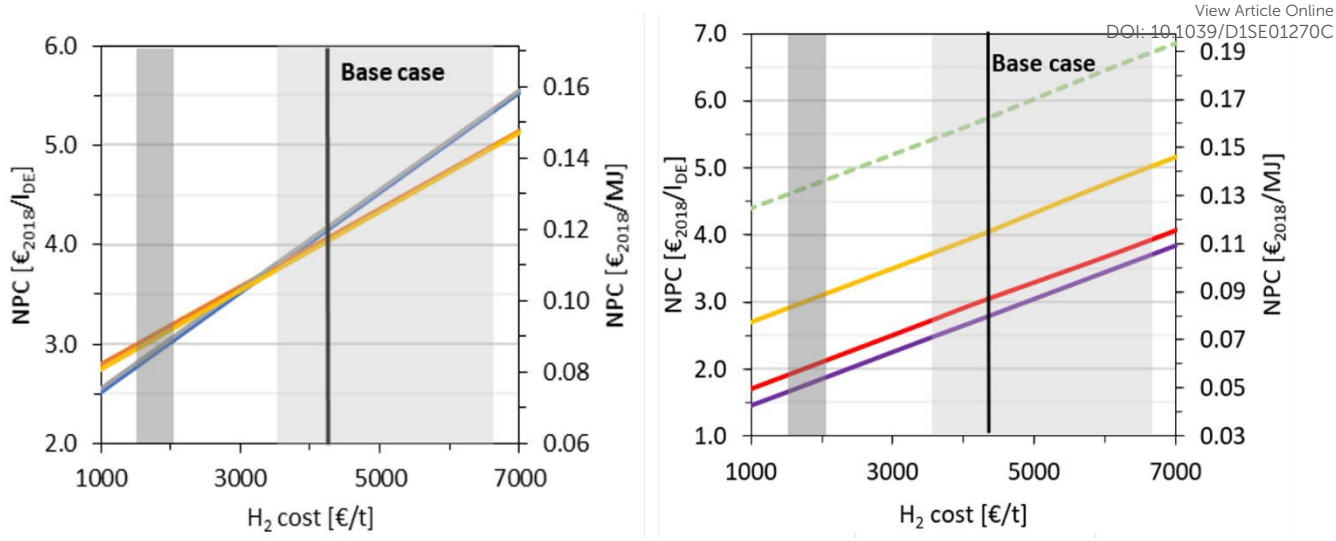

Figure 11 – (left) Dependence of NPC on the H_2 cost: P1, P2, P3, P4; dark grey shaded area: SMR cost range representing a prospective lower limit of green H_2 cost according to ref.[71], light grey shaded area: wind power-based electrolysis cost range from[71]; All other raw material costs are fixed on the base case. **(Right)** - Dependence of NPC on the H_2 and CO_2 cost: P4 at 0 €/t_{CO_2} (available CO_2 in-site), P4 at 62 €/t_{CO_2} (MEA_{2018} cost from[68]), P4 base case, P4 at 720 €/t_{CO_2} (DAC_{2018} cost from[70]); dark grey shaded area: SMR cost range representing a prospective lower limit of green H_2 cost according to ref.[71], light grey shaded area: wind power-based electrolysis cost range from[71].

Discussion of economic results

CAPEX, OPEX and NPC are calculated for the different production routes presented in this work. Main differences in the cost structure are observed for the different approaches for the FA(aqueous/anhydrous) synthesis. First, higher investment cost for heat exchangers in the FA(anhydrous) sub-process result from high reaction temperatures. This cost could be diminished by milder process conditions. Second, differences arise from the fact that in the FA(anhydrous) sub-process H_2 is formed and recycled back to the MeOH sub-process. The recycling leads to somewhat higher investment costs for compressors, but on the other hand higher H-efficiency and consequently lower H_2 costs. These savings in OPEX, which have by far the higher impact to the NPC, exceed the additional CAPEX significantly. Nevertheless, no significant differences in the overall NPC of the different routes are obtained over the whole considered parameter ranges. As a result, no route is clearly preferable from an economic point of view. A preference could at the most result from weighing up the different relations of CAPEX and OPEX resulting from the different FA sub-processes.

To the best of our knowledge, there is one peer-reviewed study in the literature conducting a techno-economic assessment of OME_{3-5} production from H_2 and CO_2 as feedstock.[40] Other publications deal with OME production from biomass[86,87] or MeOH[88,89] as feedstock and are not directly comparable to this work.

In the study of Schemme et al.[40] production routes of different oxygenated alternative fuels are studied analyzing the process efficiencies and production cost. The methodology for the economic evaluation and system boundaries are similar to the approach applied in this work. Hence, a comparison between the economic results from Schemme et. al.[40] and this work was carried out. In order to achieve a comparable data basis, the framework assumptions from Schemme et. al.[40] were applied as far as possible to the model in this work. This was mainly the case for the base year, interest rate and LHV_{OME3-5} as well as CO_2, H_2, steam and electricity cost.

Primarily, no adaptions could be made for the plant capacity, CO_2 feed conditions, cooling water and steam conditions, compressor and pump efficiencies and pressure losses. A detailed comparison of the assumptions of Schemme et al.[40] and this work and the results of the comparative calculations are given in the ESI. Applying the assumptions made in Schemme et. al.[40] to the model from this work results in NPC of 3.67 €/l_{DE} for route P1 compared to 3.46 €/l_{DE} obtained by Schemme et al.[40] ("Route A" in[40]), which corresponds to a deviation of 6 %. Hence, an agreement of the NPC of Route P1 can be stated in the error range of the calculations. Moreover, it can be concluded that the novel OME production routes P2 to P4 studied in this work are at least competitive to the TRI routes ("Route B" and "Route C") considered in Schemme et. al..[40]

Carbon footprint evaluation

Contribution analysis base case

In the base case year 2018, the carbon footprints of the process routes P1 and P3 are around 0.35 kg CO_2-eq./MJ and thus significantly higher than the carbon footprints of P2 and P4 with about 0.30 kg CO_2-eq./MJ (Figure 12 and in the ESI). We therefore compare hotspots in the OME_{3-5} supply chain exemplary for P3 and P4 (Figure 12) in the proceeding contribution analysis.

The carbon footprints of OME_{3-5} production are mostly driven by H_2 and CO_2 supply for both routes P3 and P4 as shown in Figure 12. Most emissions arise from H_2 supply, which is produced by electrolysis via today's electricity mix in the base case. Note that in P4 the H_2 supply contributes less to the carbon footprint than in P3 (Figure 12) since P4 requires 20 % less H_2 per kg OME_{3-5} than P3. The environmental credit, i.e., avoided burden, for utilized CO_2 strongly reduces the carbon footprint of both P3 and P4. However, in P4 the

View Article Online
DOI: 10.1039/D1SE01270C

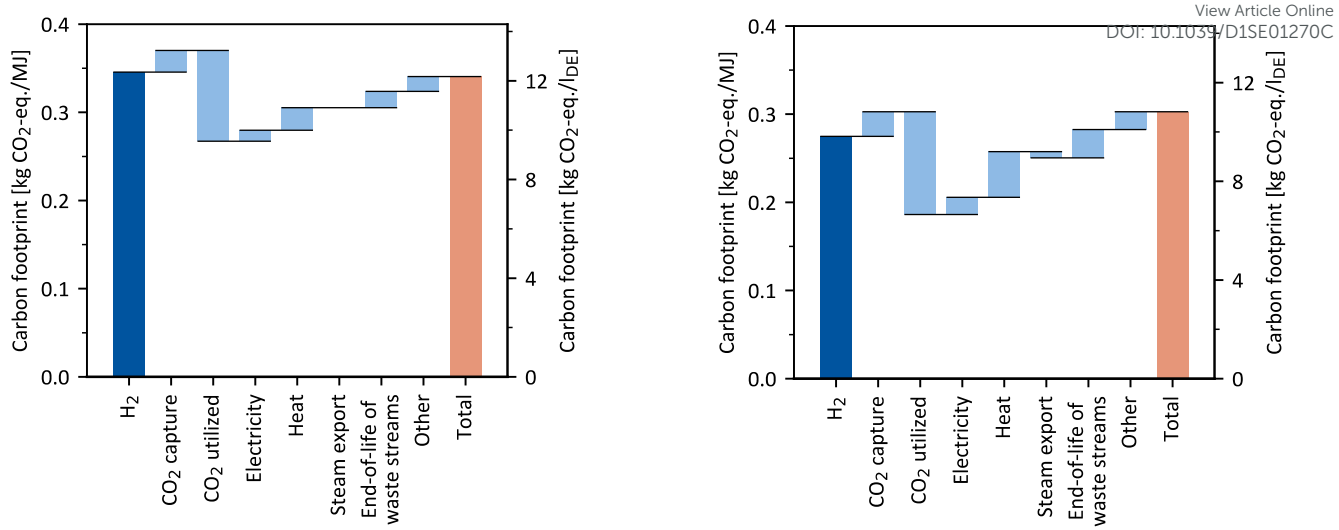

Figure 12 – Contribution analysis of the carbon footprint of the OME_{3-5} routes P3 (left) and P4 (right) for year 2018. The left y-axis shows the carbon footprint in kg CO_2- eq./MJ, while the right y-axis additionally indicates results in kg CO_2-eq./l_{DE}. The end-of-life of waste streams considers CO_2 in the exhaust gas and carbon carriers in the wastewater. Minor emissions due to wastewater treatment and the supply of cooling water, nitrogen, and compressed air are summarized as "other".

environmental credit for CO_2 utilization is higher than that of P3, since P4 requires 13 % more CO_2 per kg of produced OME_{3-5}, due to the lower carbon selectivity towards OME_{3-5} in comparison to P3. The higher amount of utilized CO_2 in P4 is thus converted into more carbon carriers in waste streams, i.e., wastewater and exhaust gas (Figure 12).

Although P4 is credited for its steam export, the heat supply in P4 contributes roughly twice as much to the carbon footprint as in P3 (Figure 12). In contrast to P3, P4 additionally requires high-temperature heat above 250 °C that is supplied electricity-based via electrode boiler.

Overall, the carbon footprint depends strongly on the carbon footprint of electricity supply if electricity-based H_2 and high-temperature heat are used. Therefore, we also investigated the influence of the carbon footprint of electricity supply on the carbon footprint of the OME_{3-5} product for all four process routes in a sensitivity analysis.

Sensitivity analysis for carbon footprint of electricity supply

In this sensitivity analysis, the carbon footprint of OME_{3-5} is minimized in a supply chain optimization as function of the carbon footprint of electricity supply, see Figure 13. For the supply chain optimization, conventional, fossil-based H_2 and high-temperature heat supply via steam methane reforming[90] and natural gas boiler[82], respectively, are included as alternatives to the PtX technologies electrolysis and electrode boiler of the base case. The tipping point between a fossil-based and PtX supply chain is reached at a carbon footprint of electricity supply of 220 g CO_2-eq./kWh_{el}. Above 220 g CO_2-eq./kWh_{el}, the supply chain optimization results in fossil-based H_2 and high-temperature heat supply since a PtX supply chain would result in a way larger carbon footprint (Figure 13, grey dotted lines).

In contrast, H_2 and high-temperature heat are supplied by PtX technologies below 220 g CO_2-eq./kWh_{el}. With an electricity carbon footprint below 56 to 68 g CO_2-eq./kWh_{el}, the production of OME_{3-5} is carbon negative. Please note that this negative carbon footprint only considers the system boundaries of OME_{3-5} production; the combustion of OME_{3-5} of course releases CO_2, making the entire life cycle of OME_{3-5} as carbon neutral at best in a complete WtW (cradle-to-grave) scope. When wind power is used for electricity supply, the carbon footprints of the OME_{3-5} production are about -36 g CO_2-eq./MJ, which is in good agreement with the results of Hank et al.[10] for low-carbon electricity supply. With today's power grid mix, a fossil-based OME_{3-5} supply chain would thus be more environmentally friendly in terms of the carbon footprint. Overall, the OME_{3-5} routes P2 and P4 have the lowest carbon footprint independent of the carbon footprint of electricity supply.

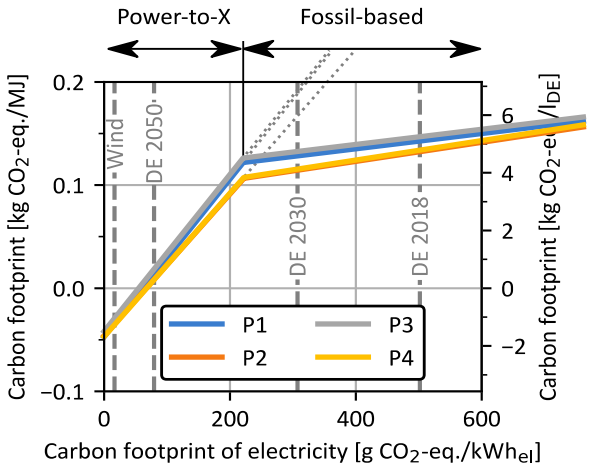

Figure 13 - The carbon footprint of all four OME_{3-5} process routes as function of the carbon footprint of electricity supply for the base case. The left y-axis shows the carbon footprint in kg CO_2-eq./MJ, while the right y-axis additionally indicates results in kg CO_2-eq./l_{DE}. Wind: wind power, DE 2018/2030/2050: German power grid mix 2018/2030/2050.[68]

Sensitivity analysis for carbon footprint of CO_2 and H_2 supply

The sensitivity of the OME_{3-5} carbon footprint towards the supply of both raw materials CO_2 and H_2 is also investigated. In case of the sensitivity analysis for CO_2 supply (Figure 14), DAC (light grey) and MEA cement (dark grey) are analysed for the years 2018 and 2050, in accordance to the generic process data of the FfE.[81] The processes P2 and P4 yield lower carbon footprints than P1 and P3 irrespective of the CO_2 supply.

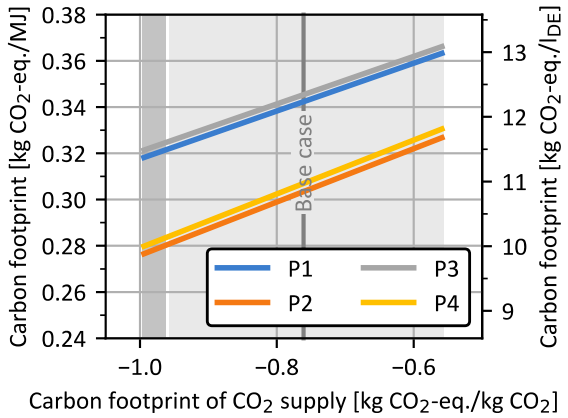

Figure 14 - The carbon footprint of all four OME_{3-5} process routes as function of the carbon footprint of CO_2 supply. The left y-axis shows the carbon footprint in kg CO_2-eq./MJ, while the right y-axis additionally indicates results in kg CO_2-eq./l_{DE}. The shaded areas indicate the carbon footprint ranges of CO_2 supply from DAC (light grey) and MEA cement (dark grey) for the years 2018 and 2050.[68]

In case of the sensitivity analysis for H_2 supply (Figure 15), generic process data for H_2 supply via electrolysis of the FfE is considered for the years 2018 (light grey) and 2050 (dark grey). With the generic process data for 2018 (light grey), the processes P2 and P4 yield the lowest carbon footprints. In contrast, when the generic process data for 2050 (dark grey) or SMR is considered, the processes P1 and P3

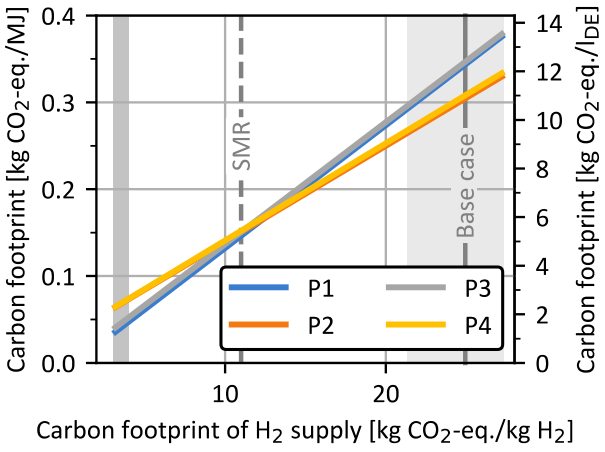

Figure 15 - The carbon footprint of all four OME_{3-5} process routes as function of the carbon footprint of H_2 supply. The left y-axis shows the carbon footprint in kg CO_2-eq./MJ, while the right y-axis additionally indicates results in kg CO_2-eq./l_{DE}. The shaded areas indicate the carbon footprint ranges of H_2 supply for the years 2018 (light grey) and 2050 (dark grey).[68] SMR: Steam methane reforming.

have lower carbon footprints than P2 and P4. With such a clean H_2 supply in 2050, the higher heat consumption of P2 and P4 becomes more decisive and leads to the higher carbon footprints of both processes in this case.

In the ESI, we additionally present sensitivity analyses for the carbon footprint of high-temperature heat supply as well as the environmental credit, i.e., avoided burden, for steam exports. The additional sensitivity analyses show that the process routes P2 and P4 yield the lower carbon footprints compared to the process routes P1 and P3 irrespective of the considered ranges of high-temperature heat supply and the environmental credit for steam exports.

Technology Readiness Level (TRL)

The TRLs assigned to the five individual sub-processes and the entire process routes P1 to P4 are shown in Table 8.

Table 8: TRL results of the sub-processes and P1 to P4.

Sub-Process	**TRL**
MeOH	9
FA(aqueous)	9
FA(anhydrous)	3-4
OME_1	9
OME_{3-5}	3-4
Total Process	
P1	3-7
P2	3-5
P3	3-8
P4	3-6

The MeOH sub-process based on H_2 and CO_2 feedstocks exists in large scale.[91] Hence, it has a TRL of 9. Identical assumptions were made by Schemme et. al.[40], also Bardow et. al.[92] cites a high TRL for this technology.

On the one hand, the FA(aqueous) sub-process also exists in large scale.[60] Hence, it has a TRL of 9. On the other hand, the FA(anhydrous) sub-process requires more research and demonstration steps to achieve the same TRL. In fact, the proof of concept was validated in several laboratory experiments.[42,62,93] However, apart from these studies, to the best of our knowledge, long-term experiments and scale-up plants have not been implemented yet. Hence, a TRL of 3-4 was assigned to this sub-process.

The OME_1 sub-process has been investigated by Drunsel et al. working on a laboratory scale distillation column.[63,94] In addition, a plant was commissioned which produces OME_1 in large-scale following the process concept of Drunsel et al.. Hence, it has a TRL of 9.[95,96] Schemme et. al.[40] also investigated the sub-process assuming a TRL of at least 5.

Different feedstocks are used for the OME_{3-5} sub-process, resulting in the need for adjustments particularly for the reactor, distillation columns and the H_2O separating process unit. However, previous studies have been conducted with regard to reaction, distillation and H_2O separation for specific mixtures, some of which are very similar to the mixtures assessed in this work and a demonstration plant[97] was built and commissioned in the scope of the NAMOSYN project. Therefore, the TRL was assumed to be 3-4. If

View Article Online
DOI: 10.1039/D1SE01370G

the demonstration plan shows promising results during long-term test runs regarding the performance of the critical process components the TRL can be assigned higher values.

The TRL for P1-P4 is presented in two ways. The first number indicates the lowest TRL of the considered sub-processes and is therefore equally 3 for all four process routes. Since this only shows the main hurdle of the entire process chain but does not show advantages of individually sub-processes the second number presents the mean TRL of the sub-processes. This is by far higher for all four process routes and a difference between P1 and P3 with the TRL 7 and 8 in comparison to P2 and P4 with the TRL 5 and 6. This is a result of the low TRL of the FA(anhydrous) sub-process in comparison to the FA(aqueous) sub-process. Due to the beneficial results of P2 and P4 regarding process efficiency and carbon footprint further investigations to improve the TRL of FA(anhydrous) should be carried out.

An overview of the process evaluation criteria for the considered processes in web diagrams for the years 2018, 2030 and 2050 is available in ESI figures S12-14.

6. Conclusions

Based on a standardized and validated modelling and simulation methodology implemented in Aspen Plus®, four different process routes for the production of OME_{3-5} were evaluated considering techno-economic and carbon footprint. The evaluated processes are based on scalable technologies that have the potential to achieve a feasible large-scale OME production. The feedstock for all four routes P1-P4 are CO_2 and H_2 to enable a sustainable production of the first intermediate product MeOH. Different sub-processes follow to prepare the intermediates for the OME_n synthesis, i.e. FA(aqueous) with MeOH for P1, FA(anhydrous) with MeOH for P2, FA(aqueous) with OME_1 for P3 and FA(anhydrous) with OME_1 for P4. Subsequent OME_{3-5} are synthesized and purified in the scale of 100 kt OME_{3-5} per year. Base case was considered under the German boundary conditions for the year 2018. All the processes were energy integrated along the process chain starting from H_2 and CO_2 with the target of maximizing the energy recovery. Based on the material and heat balance results, the overall energy efficiency evaluated for the different processes varied between ca. 50 – 55 %. Processes based on anhydrous FA (P2 and P4) showed a trend of higher energy efficiency due to the reutilization of the H_2 by-product from the MeOH endothermic dissociation reaction in the MeOH synthesis loop. From the economic point of view, the calculated NPC under base case conditions (cost of H_2 of 4,241 €/t_{H2} and cost of CO_2 of 309 €/t_{CO2}) amount to 4.14 €$_{2018}$/l_{DE} for P1, 4.05 €$_{2018}$/l_{DE} for P2, 4.18 €$_{2018}$/l_{DE} for P3 and 4.05 €$_{2018}$/l_{DE} for P4. No significant differences in the overall NPC of the different routes are obtained over the whole considered parameter ranges. This is due to a trade-off between the CAPEX and OPEX that occurred due to lower cost of feedstock for the anhydrous FA based process P2 and P4, while having higher CAPEX mainly due to the high temperature endothermic methanol dissociation reaction at low MeOH concentrations. The high dependency of the NPC on the CO_2 and H_2 costs is illustrated using sensitivity analysis. In the case of CO_2 cost variation (at H_2 base case cost), NPC of OME between 3.0 €/l_{DE} and 5.8 €/l_{DE} are obtained, while the variation of the H_2 price (at CO_2 base case cost) leads to 2.8 to 5.4 €/l_{DE} of NPC. A combination of OME production based on CO_2 point source feedstock cost and H_2 cost provisioned future production using cheap renewable electricity (at H_2 price of ≤ 2,438 €/t from AEL in 2050 and CO_2 price of ≤ 62 €/t from MEA, cement) can significantly reduce the costs for sustainable OME production at ≤ 2.33 €/l_{DE}. In case of CO_2 feedstock available onsite at no price, OME production cost under 2 €/l_{DE} can be achieved with H_2 produced under favored conditions at ≤ 2,000 €/t_{H2}.

The carbon footprints of OME_{3-5} production are mostly driven by H_2 and CO_2 supply for both routes anhydrous (P4) and aqueous FA (P3) based**.** In the base case at the year 2018, the carbon footprints of the process routes P1 and P3 are around 0.35 kg CO_2-eq./MJ and thus significantly higher than the carbon footprints of P2 and P4 with about 0.30 kg CO_2-eq./MJ. This is a result of the lower H_2 demand including the anhydrous FA production. The environmental credit, i.e., avoided burden, for CO_2 supply strongly reduces the carbon footprint of all process routes especially P4 since P4 requires 20 % less H_2 per kg OME_{3-5} than P3. However, in P4 the environmental credit for CO_2 utilization is higher than that of P3, since P4 requires 13 % more CO_2 per kg of produced OME_{3-5}, due to the lower C-selectivity towards OME_{3-5} in comparison to P3. For carbon footprint of the electricity supply of 220 g CO_2-eq./kWh_{el}, the PtX supply chain has a smaller carbon footprint than a fossil-based one. If wind power is used for the electricity supply, the carbon footprints of the OME_{3-5} production are about -36 g CO_2-eq./MJ, which is in good agreement with literature results[10] for low-carbon future electricity supply. Today's German power grid mix_{2018} is not suitable to improve the carbon footprint of the OME_{3-5} production and high penetration of renewable energy generators is indeed for sustainable production.

Overall, the routes P2 and P4 have the lowest carbon footprint independent of the carbon footprint of the electricity supply. Based on sensitivity analysis with a future scenario for the German electricity mix, the carbon footprint of promising OME production routes like P4 can reach 0.29 kg CO_2-eq./l_{DE} showing the opportunity of a sustainable production of OME. The TRL of the considered processes were evaluated in a conservative and optimistic manner at 3 – 7 based on experimental developments for critical process components of the OME value chain.

In the light of the previous results, there is generally no significant economic difference for the analysed OME production routes considered in this work. The overall energy efficiency of the considered processes however shows a positive tendency to anhydrous FA based routes which are still under research and development. An important lever to enhance the processes' energy efficiency, is to reduce energy losses by valorising low temperature excess heat through usage in external processes. A big share of the excess heat is still at useful temperature levels considering the usage of heat pump technology, an approach that is under investigation. This strategy is deciding in the context of PtX processes where the production most probably will take place where cheap renewable electricity is abundant. This will reduce the supply of external utility streams and can reflect positively on the NPC.

View Article Online
DOI: 10.1039/D1SE01270C

Since the main driver of the production costs is the feedstock (H_2 and CO_2) with almost 74 % of the NPC, the measures to create an economical frame for sustainable OME as neat fuel or a blend is significantly dependent on the H_2 production at areas with low levelized costs of electricity and with low costs for CO_2. The carbon footprint evaluation shows the potential of the environmental credit of OME production processes which can reflect on lower production costs when a WtW system boundary is considered. Monetary frames as H_2 global‡ from the federal German government and the modifications in REDII§ on the European level, to include awarding systems and enhance the market introduction for sustainable fuels which lead to CO_2 avoidance is one of the main levers for the realization of a large-scale production of these fuels. The techno-economic and carbon footprint potentials of OME large-scale production processes in Germany and worldwide based on sensitivity analysis presented in this work emphasize the potential of OME as important constituent in a sustainable future mobility sector.

Author Contributions

The process modelling and simulation and the subsequent technical evaluation is done by the Fraunhofer Institute for Solar Energy Systems ISE. KIT supported this work by evaluating the technological concepts and comparing it to the published state of the art. The cost estimation and subsequent economic evaluation is done by the DLR. The carbon footprint estimation and subsequent evaluation is done by the LTT of the RWTH Aachen University. TUM contributed to the conception, data analysis, critical revision for important content.

Conflicts of interest

The authors declare no competing financial interest.

Acknowledgement

The authors gratefully acknowledge funding by the German federal ministry of education and research (BMBF) within the NAMOSYN project “Sustainable mobility due to synthetic fuels”.
Franz Mantei also gratefully acknowledge the German federal environmental foundation (DBU) funding provided for his Dissertation.

Nomenclature

Abbreviations

Abbreviations	Full Name
ACC	Annual capital cost
AEL	Alkaline electrolysis
BEVs	Battery electrical vehicles
BMBF	German federal ministry of education and research
CAPEX	Capital expenditures
CCU	Carbon capture and utilization
CO	Carbon monoxide
CO_2	Carbon dioxide
COP	Coefficient of performance
CPS	Carbon from point sources
DAC	Direct air capture
DBU	German federal environmental foundation
DME	Dimethylether
EC	Equipment cost
EGR	Exhaust gas recirculation
FA	Formaldehyde
FCI	Fixed capital investment
FfE	Research centre for energy economics
fuel	Active combustion substance
H_2	Hydrogen
H_2O	Water
HF	poly(oxymethylene) hemiformals
ICEVs	Internal combustion engine vehicles
IEA	International Energy Agency
KPIs	Key performance indicators
LCA	Life cycle assessment
LCI	Life cycle inventory
LCIA	Life cycle impact assessment
LHV	Lower heating value
MEA	Mono-ethanol amine
MeOH	Methanol
MG	poly(oxymethylene) glycols
NAMOSYN	Sustainable mobility through synthetic fuels
N_2	Nitrogen
NO_x	Nitrous oxides
NPC	Net production costs
O_2	Oxygen
OME_1	Methylal
OME_n	OME of chain length n
OMEs	Poly(oxymethylene) dimethyl ethers
OPEX	Operational expenditures
$OPEX_{dir/ind}$	Direct and indirect operational expenditures
$OPEX_{R\&U}$	Raw material and utility costs
PEM	Polymer electrolyte membrane
pFA	Para formaldehyde
PtX	Power-to-x
RE	Renewable energy
SMR	Steam methane reforming
SOEC	Solid oxide electrolyser cell
TCI	Total capital investment
TEA	Techno-economic assessments
TEPET	Techno-economic process evaluation tool
TRI	Trioxane
TRL	Technology readiness level

‡ The H_2 Global is a funding concept by the federal German Government for a short-term economic market entry into international PtX projects and achieving the goals adopted in the German National Hydrogen Strategy in connection with the production of green H_2 and its import.[91]
§ Renewable Energy Directive – Recast to 2030 (REDII) 2018/2001/EU[92]
In REDII, the overall EU target for Renewable Energy sources consumption by 2030 has been raised to 32%. Member States must ensure that a minimum of 14% of the final energy consumption in the transport sector is provided by fuel suppliers from renewable sources.

UBA	German environment agency
VLLE	Vapor-liquid-liquid equilibria
WtW	Well-to-wheel

Symbols and Indices

Symbol or Indices	Name
η	Efficiency
η_{Mass}	Mass efficiency
η_c	Carbon efficiency
η_{Energy}	Process energy efficiency
n	Order of the reaction
P	Pressure
T	Temperature
h_{labor}	Employee-hours per year
%	Percentage
l_{DE}	Litre diesel equivalent

References

1. German Environment Agency - Germany remains on track in climate protection "Deutschland bleibt im Klimaschutz auf Kurs". https://www.bundesregierung.de/breg-de/aktuelles/klimaschutzziel-2020-erreicht-1876954, (last accessed June 2021).
2. European Parliament and of the Council, Regulation (EC) No 715/2007 approval of motor vehicles with respect to emissions from light passenger and commercial vehicles (Euro 5 and Euro 6). http://eur-lex.europa.eu/legal-content/EN/ALL/?uri=CELEX:32007R0715, (last accessed August 2021).
3. Statistica Research Department - EU car sales: share of diesel engines 2015-2019, by country. https://www.statista.com/statistics/425113/eu-car-sales-share-of-diesel-engines-by-country/, (last accessed June 2021).
4. Statistica Research Department - EU car sales: share of diesel engines 2015-2019, by brand. https://www.statista.com/statistics/425324/eu-car-sales-share-of-diesel-engines-by-brand/, (last accessed June 2021).
5. International Energy Agency, World Energy Outlook 2020, Outlook for energy demand. https://www.iea.org/reports/world-energy-outlook-2020/outlook-for-energy-demand, (last accessed August 2021).
6. E. Jacob and W. Maus, eds., Synthetic Fuels–OME1: A Potentially Sustainable Diesel Fuel: 325-347, 35. Wiener Motorensymposium, Vienna, 2014.
7. E. Jacob and W. Maus, MTZ Worldw, 2017, **78**, 52.
8. M. Härtl, K. Gaukel, D. Pélerin and G. Wachtmeister, MTZ worldwide, 2017, **78**, 52.
9. M. Münz, A. Mokros, D. Töpfer and C. Beidl, MTZ Worldw, 2018, **79**, 16.
10. C. Hank, L. Lazar, F. Mantei, M. Ouda, R. J. White, T. Smolinka, A. Schaadt, C. Hebling and H.-M. Henning, Sustainable Energy Fuels, 2019, **3**, 3219.
11. H. Chen, R. Huang, H. Huang, M. Pan and W. Teng, Applied Thermal Engineering, 2019, **150**, 591.
12. B. Lumpp, D. Rothe, C. Pastötter, R. Lämmermann and E. Jacob, MTZ Worldw, 2011, **72**, 34.
13. H. Liu, Z. Wang, J. Wang, X. He, Y. Zheng, Q. Tang and J. Wang, Energy, 2015, **88**, 793.
14. S. E. Iannuzzi, C. Barro, K. Boulouchos and J. Burger, Fuel, 2017, **203**, 57.
15. J. Liu, H. Wang, Y. Li, Z. Zheng, Z. Xue, H. Shang and M. Yao, Fuel, 2016, **177**, 206.
16. J. Liu, P. Sun, H. Huang, J. Meng and X. Yao, Applied Energy, 2017, **202**, 527.
17. A. Omari, B. Heuser, S. Pischinger and C. Rüdinger, Applied Energy, 2019, **239**, 1242.
18. T. Popp, R. Lechner, M. Becker, M. Hebauer, N. O'Connell and M. Brautsch, Applied Thermal Engineering, 2019, **153**, 483.
19. Y. R. Tan, M. L. Botero, Y. Sheng, J. A. Dreyer, R. Xu, W. Yang and M. Kraft, Fuel, 2018, **224**, 499.
20. J. Tian, Y. Cai, X. Pu, L. Gu, Y. Shi, Y. Cui and R. Fan, Chem. Pap., 2018, **134**, 993.
21. Z. Wang, H. Liu, J. Zhang, J. Wang and S. Shuai, Energy Procedia, 2015, **75**, 2337.
22. H. Yang, X. Li, Y. Wang, M. Mu, X. Li and G. Kou, Aerosol Air Qual. Res., 2016, **16**, 2560.
23. Y. Zhao, C. Geng, W. E, X. Li, P. Cheng and T. Niu, Scientific reports, 2021, **11**, 9514.
24. Y. Zhao, Y. Xie, X. Wang, Z. Li, T. Niu and S. Liu, Energy Convers. Mgmt., 2020, **225**, 113489.
25. Josefine Preuß, Karin Munch and Ingemar Denbratt, Fuel, 2021, **303**, 121275.
26. Dominik Pélerin, Kai Gaukel, Martin Härtl, Eberhard Jacob and Georg Wachtmeister, Fuel, 2020, **259**, 116231.
27. P. Dworschak, V. Berger, M. Härtl and G. Wachtmeister in SAE Technical Paper Series, SAE International400 Commonwealth Drive, Warrendale, PA, United States, 2020.
28. S. Deutz, D. Bongartz, B. Heuser, A. Kätelhön, L. Schulze Langenhorst, A. Omari, M. Walters, J. Klankermayer, W. Leitner, A. Mitsos, S. Pischinger and A. Bardow, Energy Environ. Sci., 2018, **11**, 331.
29. M. Kass, M. Wissink, C. Janke, R. Connatser and S. Curran in SAE Technical Paper Series, SAE International400 Commonwealth Drive, Warrendale, PA, United States, 2020.
30. Dr.-Ing. M. Härtl and G. Wachtmeister, Methanol derived synthetic fuels for diesel and spark ignited engines. 4th Methanol Technology and Policy Commercial Congress, Frankfurt an Main, 2017.
31. T. Wilharm and E. Jacob, First steps towards the market launch of OME diesel 4th Methanol Technology and Policy commercial congress, Frankfurt an Main, 2017.

View Article Online
DOI: 10.1039/D1SE01270C

32. Dr. Jens Perner, Theresa Steinfort, Frontier Economics DER "EFFIZIENZBEGRIFF" IN DER KLIMAPOLITISCHEN DEBATTE ZUM S, 2020.
33. C. J. Baranowski, A. M. Bahmanpour and O. Kröcher, Applied Catalysis B: Environmental, 2017, **217**, 407.
34. D. N. D. Moulton, Diesel Fuel having improved qualities and method of forming(US5746785 A), 1998.
35. D. SanFilippo, R. Patrini and M. Marchionna, Use of an oxygenated product as a substitute of gas oil in diesel engines(EP1422285 A1), 2004.
36. K. D. Vertin, J. M. Ohi, D. W. Naegeli, K. H. Childress, G. P. Hagen, C. I. McCarthy, A. S. Cheng and R. W. Dibble, Methylal and Methylal-Diesel Blended Fuels for Use in Compression-Ignition Engines, 1999.
37. L. Lautenschütz, Neue Erkenntnisse in der Syntheseoptimierung oligomerer Oxymethylendimethylether aus Dimethoxymethan und Trioxan, Inaugural-Dissertation, Ruprecht-Karls-Universität Heidelberg, 2015.
38. K. Hackbarth, P. Haltenort, U. Arnold and J. Sauer, Chem. Ing. Tech., 2018, **90**, 1520.
39. J. Burger, E. Ströfer and H. Hasse, Chemical Engineering Research and Design, 2013, **91**, 2648.
40. S. Schemme, J. L. Breuer, M. Köller, S. Meschede, F. Walman, R. C. Samsun, R. Peters and D. Stolten, International Journal of Hydrogen Energy, 2020, **45**, 5395.
41. D. Bongartz, J. Burre and A. Mitsos, Industrial & Engineering Chemistry Research, 2019.
42. M. Ouda, F. Mantei, K. Hesterwerth, E. Bargiacchi, H. Klein and R. J. White, React. Chem. Eng., 2018, 676.
43. M. Held, Y. Tönges, D. Pélerin, M. Härtl, G. Wachtmeister and J. Burger, Energy Environ. Sci., 2019, **12**, 1019.
44. C. J. Baranowski, M. Roger, A. M. Bahmanpour and O. Kröcher, ChemSusChem, 2019. 10.1002/cssc.201901814.
45. N. Schmitz, J. Burger and H. Hasse, Industrial & Engineering Chemistry Research, 2015, **54**, 12553.
46. N. Schmitz, E. Ströfer, J. Burger and H. Hasse, Industrial & Engineering Chemistry Research, 2017, **56**, 11519.
47. N. Schmitz, C. F. Breitkreuz, E. Ströfer, J. Burger and H. Hasse, Chemical Engineering and Processing - Process Intensification, 2018. 10.1016/j.cep.2018.06.012.
48. N. Schmitz, C. F. Breitkreuz, E. Ströfer, J. Burger and H. Hasse, Journal of Membrane Science, 2018, **564**, 806.
49. D. Oestreich, L. Lautenschütz, U. Arnold and J. Sauer, Chem. Eng. Sci., 2017, **163**, 92.
50. I. Hahnenstein, H. Hasse and G. Maurer, Industrial & Engineering Chemistry Research, 1994, **33**, 1022–1029.
51. I. Hahnenstein, M. Albert, H. Hasse, C. G. Kreiter and G. Maurer, Ind. Eng. Chem. Res., 1995, **34**, 440.
52. M. Maiwald, H. H. Fischer, M. Ott, R. Peschla, C. Kuhnert, C. G. Kreiter, G. Maurer and H. Hasse, Ind. Eng. Chem. Res., 2003, **42**, 259.
53. M. Maiwald, T. Grützner, E. Ströfer and H. Hasse, Analytical and Bioanalytical Chemistry, 2006, **385**, 910.
54. G. Maurer, AIChE J., 1986, **32**, 932.
55. W. Maus, ed., Zukünftige Kraftstoffe, Springer Berlin Heidelberg, Berlin, Heidelberg, 2019.
56. F. Nestler, M. Krüger, J. Full, M. J. Hadrich, R. J. White and A. Schaadt, Chem. Ing. Tech., 2018, **90**, 1409.
57. A. Otto, Chemische, verfahrenstechnische und ökonomische Bewertung von Kohlendioxid als Rohstoff in der chemischen Industrie, 2015.
58. D. Bongartz, L. Doré, K. Eichler, T. Grube, B. Heuser, L. E. Hombach, M. Robinius, S. Pischinger, D. Stolten, G. Walther and A. Mitsos, Applied Energy, 2018, **231**, 757.
59. F. Nestler, A. R. Schütze, M. Ouda, M. J. Hadrich, A. Schaadt, S. Bajohr and T. Kolb, Chem. Eng. J., 2020, **394**, 124881.
60. A. W. Franz, H. Kronemayer, D. Pfeiffer, R. D. Pilz, G. Reuss, W. Disteldorf, A. O. Gamer and A. Hilt in Ullmann's Encyclopedia of Industrial Chemistry, ed. Wiley-VCH, Wiley-VCH Verlag GmbH & Co. KGaA, Weinheim, Germany, 2012.
61. S. Su, M. R. Prairie and A. Renken, Applied Catalysis A: General, 1993, **95**, 131.
62. J. Sauer and G. Emig, Chem. Eng. Technol., 1995, **18**, 284.
63. J.-O. Drunsel, Entwicklung von Verfahren zur Herstellung von Methylal und Ethylal, Scientific Report Series, 2012.
64. R. W. Baker, Membrane technology and applications, J. Wiley, Chichester, New York, 2010.
65. M. S. Peters, K. D. Timmerhaus and R. E. West, Plant design and economics for chemical engineers, McGraw-Hill, Boston, 2003.
66. F. G. Albrecht, D. H. König, N. Baucks and R.-U. Dietrich, Fuel, 2017, **194**, 511.
67. S. Brynolf, M. Taljegard, M. Grahn and J. Hansson, Renewable and Sustainable Energy Reviews, 2018, **81**, 1887.
68. J. Prause, M. Raab, R.-U. Dietrich (2020), private communication. Framework assumptions TEA, Begleitforschung Energiewende im Verkehr (BEniVer).
69. H. Naims, Environmental science and pollution research international, 2016, **23**, 22226.
70. K. Z. House, A. C. Baclig, M. Ranjan, E. A. van Nierop, J. Wilcox and H. J. Herzog, Proceedings of the National Academy of Sciences of the United States of America, 2011, **108**, 20428.
71. V. Bouillon-Delporte, J. C., N. Brahy, Clean Hydrogen - Monitor 2020, Hydrogen Europe Intelligence Departement., 2020.
72. R. Edwards, S. Godwin, H. Hamje, H. Hass, A. Krasenbrink, J.-F. Larivé, L. Lonza, H. Maas, R. Nelson, A. Reid, D. Rickeard, K. D. Rose and W. Weindorf, Well-to-wheels report version 4.a: JEC well-to-wheels analysis well-to-wheels analysis of future automotive fuels and powertrains in the European context, Publications Office of the European Union, Luxembourg, 2014.
73. D. R. Woods, Rules of thumb in engineering practice, Wiley-VCH, Weinheim, 2007.
74. Ullmann's Encyclopedia of Industrial Chemistry, Wiley-VCH Verlag GmbH & Co. KGaA, Weinheim, Germany, 2012.
75. M. E. Boot-Handford, J. C. Abanades, E. J. Anthony, M. J. Blunt, S. Brandani, N. Mac Dowell, J. R. Fernández, M.-C.

Ferrari, R. Gross, J. P. Hallett, R. S. Haszeldine, P. Heptonstall, A. Lyngfelt, Z. Makuch, E. Mangano, R. T. J. Porter, M. Pourkashanian, G. T. Rochelle, N. Shah, J. G. Yao and P. S. Fennell, Energy Environ. Sci., 2014, **7**, 130.
76. M. Fasihi, O. Efimova and Ch. Breyer, Journal of Cleaner Production, 2019, **224**, 957.
77. L. J. Müller, A. Kätelhön, S. Bringezu, S. McCoy, S. Suh, R. Edwards, V. Sick, S. Kaiser, R. Cuéllar-Franca, A. El Khamlichi, J. H. Lee, N. v. d. Assen and A. Bardow, Energy Environ. Sci., 2020, **13**, 2979.
78. I. Kolakovic, H. Vreeswijk, F. Iscru, Labour costs in the EU, 60/2018, Eurostat, Luxembourg, 2018.
79. International Organization for Standardization, DIN EN ISO 14040: Environmental Management: Life Cycle Assessment: Principles and Framework, 2006.
80. International Organization for Standardization, DIN EN ISO 14044: Environmental Management: Life Cycle Assessment: Requirements and Guidelines, 2006.
81. Forschungsstelle für Energiewirtschaft e.V. (FfE), Ökobilanzen synthetischer Kraftstoffe: Methodikleitfaden. 2020 [Research Center for Energy Economics (FfE), Life Cycle Assessments of Synthetic Fuels: Methodology Guide. 2020].
82. G. Wernet, C. Bauer, B. Steubing, J. Reinhard, E. Moreno-Ruiz and B. Weidema, Int J Life Cycle Assess, 2016, **21**, 1218.
83. 7th Energy Research Programme of the Federal Government - Research for an environmentally-friendly, reliable and affordable energy supply. https://www.bmwi.de/Redaktion/EN/Artikel/Energy/research-for-an-ecological-reliable-and-affordable-power-supply.html, (last accessed June 2021).
84. H. Sperber, Chem. Ing. Tech., 1969, **41**, 962.
85. Felix Schorn, Janos L. Breuer, Remzi Can Samsun, Thorsten Schnorbus, Benedikt Heuser, Ralf Peters and Detlef Stolten, Advances in Applied Energy, 2021, **3**, 100050.
86. A. Zimmermann, R. Schomäcker, E. Gençer, F. O'Sullivan, K. Armstrong, P. Styring and S. Michailos, Global CO2 Initiative Complete Oxymethylene Ethers Study 2018, 2019.
87. A. O. Oyedun, A. Kumar, D. Oestreich, U. Arnold and J. Sauer, Biofuels, Bioprod. Bioref., 2018, **89**, 3315.
88. M. Martín, J. Redondo and I. E. Grossmann, ACS Sustainable Chem. Eng., 2020, **8**, 6496.
89. N. Schmitz, J. Burger, E. Ströfer and H. Hasse, Fuel, 2016, **185**, 67.
90. S. Deutz and A. Bardow, Nat Energy, 2021, **6**, 203.
91. FReSMe project - From Residual Steel Gases to Methanol. https://www.carbonrecycling.is/news-media/fresme-project-reaches-final-milestone-from-blast-furnace-waste-emissions-to-ferry-fuel, (last accessed August 2021).
92. K. Roh, A. Bardow, D. Bongartz, J. Burre, W. Chung, S. Deutz, D. Han, M. Heßelmann, Y. Kohlhaas, A. König, J. S. Lee, R. Meys, S. Völker, M. Wessling, J. H. Lee and A. Mitsos, Green Chem, 2020, **22**, 3842.
93. S. Su, P. Zaza and A. Renken, Chem. Eng. Technol., 1994, **17**, 34.
94. J.-O. Weidert, J. Burger, M. Renner, S. Blagov and H. Hasse, Ind. Eng. Chem. Res., 2017, **56**, 575.
95. Prefere paraform, products, Dimethoxymethan (Methylal), Prefere Resins Holding GmbH. https://prefere.com/de/paraform/produkte/dimethoxymethan, (last accessed August 2021).
96. Nurluqman Suratman, INEOS Paraform starts up new methylal plant in Germany, Independent Commodity Intelligence Services, 2012. https://www.icis.com/explore/resources/news/2012/08/07/9584533/ineos-paraform-starts-up-new-methylal-plant-in-germany/, (last accessed August 2021).
97. A. Ferre, J. Voggenreiter, Y. Tönges and J. Burger, MTZ Worldw, 2021, **82**, 26.
98. Hydrogen Energy Partnerships for Climate protection and industrial growth. https://h2-global.de/, (last accessed 21.07.16).
99. European Commission, Promotion of the Use of Energy from Renewable Sources: 2018/2001/EU: REDII: 2018/2001/EU, 2018.

View Article Online
DOI: 10.1039/D1SE01270C